Environmental Earth Sciences (2023) 82:130
https://doi.org/10.1007/s12665-023-10777-7

ORIGINAL ARTICLE

Distribution, mode of occurrence, and significance of rare-earth elements in coal from Samaleswari open cast coal blocks, Odisha, India with their provenance and paleodepositional environment

Sneha Kumari[1] · Toushali Roy[1] · Saswati Chakladar[1] · Alok Kumar[1,2] · Md. Arif[1] · Ashok Mohanty[1] · Rajen Kundu[1] · Sanchita Chakravarty[1]

Received: 8 June 2022 / Accepted: 16 January 2023 / Published online: 2 March 2023

Abstract

This study aims to thoroughly examine the distribution, concentration, and occurrence of a broad selection of REEs and major elements in coal samples from Samaleswari coal block, IB valley, Odisha, India using advanced geochemical tools. A total of 85 coal samples from four boreholes were characterized using proximate analysis and calorific value measurements. The corresponding ash samples were examined using X-ray Diffraction (XRD), X-ray Fluorescence (XRF), Electron Probe Microanalyzer (EPMA), and Inductively Coupled Plasma Mass Spectrometry (ICP-MS).The coal ash samples were delineated to be rich in SiO_2 (42–65%) along with a lower proportion of Al_2O_3 (24–41%), Fe_2O_3 (5–6%), and TiO_2 (1–2%). The average concentration of REEs in the four boreholes was found to be 510 ppm, with the distribution pattern being Ce > La > Nd > Y > Pr > Sc > Sm > Gd > Dy > Er > Yb > Eu > Ho > Tb > Tm > Lu. The concentration of critical REEs varied in the range of 100–300 ppm, and outlook coefficient (C_{outl}) ranged from 0.7 to 1.0, demonstrating our coal seams' suitability as a promising source of REEs. A higher concentration of REEs in BH1 was correlated with a relatively higher proportion of apatite. The increment in REE concentration with depth was speculated to be due to their close association with hematite, especially in BH1 and BH2. A strong positive correlation of all the REEs with clay minerals and specifically TiO_2 reinstates their abundance in fine-grained clastic sedimentary rocks which are not significantly affected by weathering. Point analysis using EPMA and Scanning Electron Microscope–Energy Dispersive Analysis X-ray (SEM–EDAX) confirmed the co-existence of La, Ce, Pr, and Nd in the Fe-containing aluminosilicate matrix. In addition, the major oxide ratio and their plot entail terrestrial depositional environment in the basin during coal formation and deposited in semi-arid climatic conditions.

Keywords Samaleswari coal · Rare-earth element distribution · Pearson correlation · Geochemistry · Mineralogy · Paleodepositional conditions

Introduction

Coal is a combination of several organic and inorganic components. The inorganic constituents of the coal can often result from the deposition of sediments by fluids existing in the basin, sediment infilling during diagenesis, or input from syn-sedimentary volcanic activities (Ward 2016). The inorganic part of the coal is as important as the organic components, as it conveys crucial information about the depositional settings, the geological history of the strata, and regional tectonic movement (Wang et al. 2017). For many decades, coal has been utilized only as a fossil fuel to generate heat energy. However, recent research has proved that coal ash produced from industries and coal deposits can act as a storehouse of many economic minerals and important trace and rare-earth elements (Seredin et al. 2013; Hower et al. 2016; Ward 2016; Dai et al. 2018; Qin et al. 2018). Productive utilization of coal ash has been a persistent area of research and development (Bhattacharjee and Kandapal 2002). Coal combustion by-products are considered as alternative resources for REEs, owing to their enrichment in critical REEs and low-to-no-cost availability as waste

✉ Sanchita Chakravarty
sanchita@nmlindia.org

[1] Analytical and Applied Chemistry Division, CSIR-National Metallurgical Laboratory, Jamshedpur 831007, India

[2] Department of Geology, Faculty of Science, University of Malaya, 50603 Kuala Lumpur, Malaysia

products (Mayfield and Lewis 2013; Seredin et al. 2013; US department of energy 2017; Dai and Finkelman 2018; Sorokin et al. 2019). On an average, if coal typically contains 60 ppm of REE, a power plant ash produced from coal will have approximately 470 ppm of REEs (Seredin and Dai 2012). Consequently, utilization of coal ash waste for REE extraction, instead of augmenting mining exploration, is undoubtedly an environmentally sustainable approach. (Franus et al. 2015; Kolker et al. 2017).

Rare-earth elements are considered a critical raw material because of the large difference between global demand and their fewer resources (Franus et al. 2015). Identification of REE distribution and assessment of their possible association with other mineral oxides are crucial to improve the efficiency of their extraction. Most of the preliminary investigations on the mapping and distribution of REEs were performed in China (Zheng et al. 2007; Wang et al. 2008; Dai et al. 2016a). Subsequently, it gained a broader perspective owing to elevated demand, and research groups around the world started uncovering their own REE resources in coal deposits through distribution studies. In addition to economic importance, the distribution of rare-earth elements along with trace elements and mineralogical characterization has been provided important information about the provenance, mode of occurrence, and paleodepositional setting of the concern basin (Dai et al. 2016a, 2018; Wang et al. 2022).

Many researchers have studied rare-earth element distribution along with geochemistry and mineralogy of coal and coal-bearing strata throughout the globe (Birk and White 1991; Kortenski and Bakardjiev 1993; Seredin et al. 1996; Seredin 1998; Eskenazy 2009; Seredin et al. 2013; Dai et al. 2016a; Hower et al. 2016; Kolker et al. 2017; Dai et al. 2018; Qin et al. 2018; Sorokin et al. 2019; Tatar and Alipor-Asll 2020; Firman and Haya 2021; Wang et al. 2022). As concern to Indian coal-bearing strata, such kinds of investigations are very limited and based on sporadic samples (Saha et al. 2016, 2018; Saikia et al. 2021). Despite this, India has about 6% of the total global reserve of REEs but produces only 1% of the global supply, which is far below its actual capacity (Indian Bureau of Mines 2019). Exploration of potential geographical sources of valuable elements from coal necessitates both: (1) recognizing coals with high concentrations of REEs and then (2) formulating efficient strategies to extract the valuables. At present, even though research is targeted toward both goals; the emphasis is primarily on development of efficient extraction strategies of these elements. Therefore, the present investigation focuses on the distribution of REEs, major elements in major coalfield located at Samaleswari Open Cast Coal Block using advanced geochemical techniques. Samaleswari Coal Block belongs to IB valley Coalfield, Odisha. The total coal reserve in IB river was estimated to be 29,619.67 million tons, according to the recent statistics published by the Geological Survey of India (Geological Survey of India 2019). The knowledge of mineralogical composition (both REE and trace elements) of this particular area is crucial in terms of its further utilization for indigenous resources.

Geological setting

In the present investigation, the coal samples have been collected from the Samaleswari area, located in IB Valley Coalfield, Odisha. The IB river basin is a part of the Mahanadi Gondwana basin that lies in a major NW–SE-trending lineament extending over 150 km from Korba, Chhattisgarh, to Sambalpur, Odisha. The IB Valley Coalfield is named after a tributary of Mahanadi (Mishra et al. 2016). It consists of two sub-basins, i.e., Hingir in the north and Rampur in the south (Fig. 1), marked by a major fault (Singh et al. 2013).

The IB basin is exposed in a westerly plunging synclinal flexure in the form of a half elliptical basin closed toward the northwest. The basement is marked by Precambrian gneissic rocks exposed by the periphery of the basin (Manjrekar et al. 2006; Singh et al. 2013; Senapati and Behera 2015). The S–W boundary fault juxtaposes these Archean rocks with the younger Permian rocks. The sedimentary rocks started with the Talchir Formation, which unconformably overlies the basement, followed by the Karharbari and Barakar Formations of the Lower Permian age (Table 1). The upper Permian to lower Triassic sedimentary Formations are represented by Lower Kamathi and Upper Kamathi Formation, which are correlated with Barren Measures and Ranighanj Formation for the generalized Gondwana succession.

Samaleswari coal block is located in the Jharsuguda district with latitude 21˚46'–21˚49'N and longitude 83˚52'–83˚56'E, as depicted in Fig. 1. Four boreholes were selected from this area for the present study, each containing 3–4 seams with varying depths. The total number of coal samples collected, along with the respective depth of each borehole, is tabulated in Table 2.

Materials and methods

A total of 85 coal samples from four boreholes (BH1, BH2, BH3, and BH4) of Samaleswari Coal Block were collected for the present investigation. The collected coal samples were pulverized in a ball mill with 100% passing of -212 µm (-72 mesh) sieve prior to analysis. Proximate analysis, viz., moisture, ash, and volatile matter content, of the coal was performed using proximate analyzer as per IS 1350 (Part 1): RA 2019. The Gross Calorific Value (GCV) of coal samples was determined using Parr 6200 bomb calorimeter (Parr, USA) as per ASTM D 5865:2019. The coal ash sample was prepared by heating the coal sample

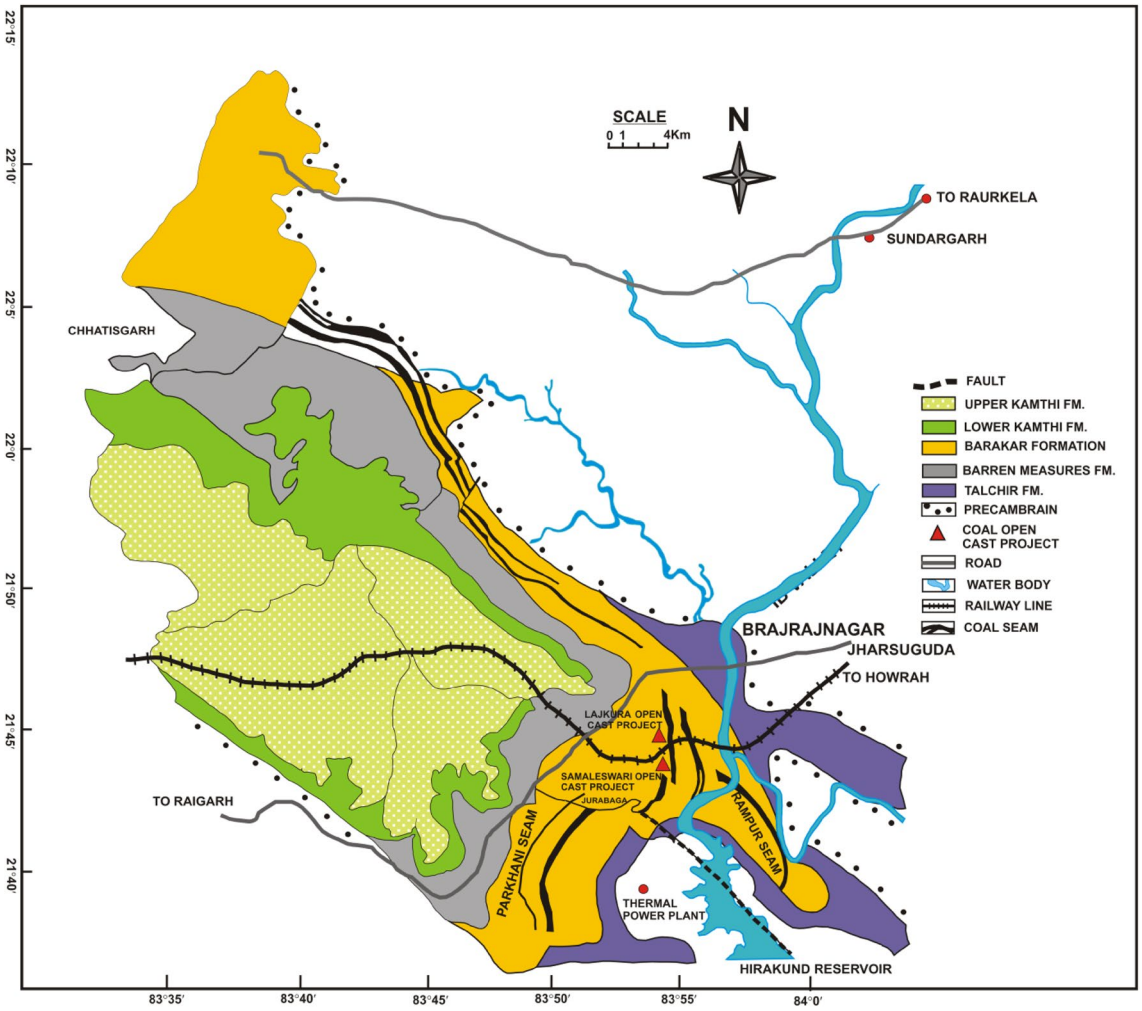

Fig. 1 Location of Samaleswari Open Cast Mines, IB valley, Odisha, India (after Senapaty and Behera 2015)

Table 1 Geological succession of the IB valley coalfield (adapted from Senapaty and Behera 2015)

Age	Formation	Lithology
Recent		Alluvium; sand, silt and clay of older alluvium, younger flood plain deposits
Sub-recent		Laterites/recent gravel and conglomerate beds
Up. Permian to lower Triassic	Kamthi (upper) = Raniganj	Conglomerates, pebbly and ferruginous sandstones
	Kamthi (lower) = Barren measures	Gray and carbonaceous shales, sandstone, clay and iron stone nodules
	Barakar	Gray sandstone, carbonaceous shale, silt stone with thick coal seams
Lower Permian	Karharbari	Black carbonaceous sandstone, pebble bed, coal seams
	Talcher	Diamictite, greenish sand stone, olive and chocolate shales
Unconformity		
Precambrian		Granite gneisses, amphibolites, etc.

in presence of air at 850 °C for 1 h in a muffle furnace as per IS:1350 (Part 1): RA 2019. Lithium metaborate and lithium tetraborate were purchased from Loba Chemie. Nitric acid (reagent grade, 65%) was procured from Rankem, India. Deionized (DI) water was produced in the lab using a Milli Q water purification system (Millipore).

The elemental composition of the selected coal ash sample was determined using X-ray fluorescence (XRF)

Table 2 Details of boreholes selected for sample collection

No. of sample	Borehole name	Depth (meter)
24	BH1	19.78–450.98
17	BH2	8.40–404.19
20	BH3	12.58–416.00
24	BH4	13.80–375.84

spectrophotometer (S8 Tiger, Bruker) using the press pellet method. Quantitative measurement of rare-earth elements in all the coal ash samples was determined using an inductively coupled plasma-mass spectrometer (ICP-MS) (Perkin Elmer, Model ELAN DRC-e with Axial Field Technology). The XRD pattern was recorded over a 2θ range of 5°- 90°, with a step size of 0.03° using Ni-filtered Cu Kα radiation. The qualitative mineralogical analysis of all acquired XRD patterns was performed using High Score plus software on the basis of JCPDS database. Point analysis of representative coal ash samples from each borehole was performed using both electron probe micro-analyzer (EPMA) (JXA 8230, JEOL) and Scanning Electron Microscopy (SEM) (FEI NOVA NANOSEM 430) using acceleration voltage of 15 kV.

Determination of total REE concentration

The total REE concentration was determined according to the protocol published previously (Banerjee et al. 2021). For each set of experiment, coal ash sample (0.1 g) was mixed with fusion mixture of lithium metaborate (0.2 g, $LiBO_2$) and lithium tetraborate (0.15 g, $Li_2B_4O_7$). The fusion mixture was thoroughly shaken to avoid lump formation during the course of reaction. The coal ash–borate mixture was then fused at 950 °C in a muffle furnace for 1 h, followed by stepwise cooling at 300 °C and then room temperature. Nitric acid solution (10%) was added to the fused sample and the resultant mixture was stirred to ensure complete dissolution. The extracted solution obtained was then transferred into a 250 ml volumetric flask and taken forward for ICP-MS analysis.

Statistical analysis methods

Box-and-whisker plot diagrams were constructed to analyze the distribution of REEs in chosen boreholes. Agglomerative hierarchical clustering (AHC) was performed between elemental oxides and REEs to establish their degree of correlation. The Pearson's concentration coefficient was used to show the interrelationship and coherence pattern among REEs of the coal ash samples which were examined.

Results and discussion

Chemical composition of coal

The results obtained for proximate analysis of the four selected boreholes (BH1, BH2, BH3, BH4) of Samaleswari Block are presented in Tables 3 and 4 and Table S-1a, b. It is evident from the tabulated results that there is a significant variation in the quality of coal samples from one borehole to another. The gross calorific values demonstrated a notable increase as we increased the depth from where the samples were collected, owing to reduction in the content of mineral matter. On the basis of the proximate analysis, the average ash content in the four boreholes ranged from 49 to 51%, fixed carbon concentration ranged from 23 to 25% and the moisture content varied from 3.8 to 5% (Table 5). The coal collected from the deepest band of each borehole demonstrated highest quality. For example, for borehole BH1, the sample collected at a depth of 450 m showed highest GCV value (5036 kcal/kg), lowest mineral matter content (31%), and lowest moisture content (3.44%). Similar observations were made for all the boreholes. The average values of all the parameters obtained in individual boreholes are tabulated in Table 5.

Major-element concentrations in coals

The chemistry of feed coal and the process parameters during its combustion largely dictates the chemical composition of the resultant coal ash. As evident from the XRF analysis, coal ash corresponding to coals of Samaleswari Block is typically comprised of the following oxides: SiO_2, Al_2O_3, Fe_2O_3, and TiO_2 in higher proportions and CaO, MgO, K_2O, P_2O_5, Na_2O, and SO_3 in minor concentration (shown in Tables 6 and 7 and Table S-2a, b). SiO_2 and Al_2O_3 were the two major oxides whose concentration varied in the range of 42–65% and 24–41%, respectively, across the four boreholes. Interestingly, Fe_2O_3 demonstrated the highest variation in concentration among the entire samples which were examined. For instance, in sample A24 (BH1), the concentration of Fe_2O_3 was only 1.08% (Table 6), whereas in sample B13 (BH2), it was present in 22.5% (Table 7). The concentration of hematite (Fe_2O_3) increased with depth, more prominently for BH1 and BH2. The increase in REE concentration could be well correlated with hematite abundance in these two boreholes (Table 6 and 7). Hematite bearing REE phases is a common occurrence in coal samples of varied geological origin (Oreskes et al. 1990; Abaka-Wood 2022). Overall, the oxides of the major elements (Si, Al, Fe, and Ti) measured up to approximately 94% of the total ash compositions, the remaining 6% being that of the minor oxides. The

Table 3 Proximate analysis of BH1 (*VM* volatile matter, *GCV* gross calorific value)

Depth (m)	Samples	Moisture (%)	Ash (%)	VM (%)	Fixed carbon (%)	GCV (kcal/kg)
19.78–30.44	A1	4.88	53.18	22.84	19.10	2725.31
51.97–53.20	A2	6.94	38.02	29.59	25.45	3835.75
92.93–95.68	A3	3.84	55.68	21.37	19.11	2660.18
108.34–112.28	A4	3.71	57.61	20.22	18.46	2500.61
116.16–118.39	A5	3.57	61.11	18.40	16.93	2176.18
120.10–121.32	A6	4.66	49.49	22.83	23.02	3149.48
139.43–140.00	A7	4.11	55.94	19.69	20.26	2585.80
142.26–143.63	A8	4.11	49.30	22.24	24.35	3246.94
152.20–153.94	A9	3.66	57.04	19.61	19.69	2552.62
162.67–164.30	A10	4.60	48.30	23.35	23.75	3226.73
206.84–207.97	A11	4.64	43.17	25.63	26.55	3718.72
216.55–219.33	A12	4.27	46.42	24.38	24.93	3461.08
275.27–303.86	A13	3.89	41.60	26.96	27.56	3994.22
311.98–315.77	A14	3.74	52.48	23.98	19.80	2978.77
316.75–323.50	A15	3.47	43.27	26.37	26.90	3909.44
311.98–323.50	A16	3.24	51.62	24.13	21.00	3131.66
372.73–377.10	A17	2.98	54.96	20.32	21.74	2864.83
380.15–381.41	A18	2.88	54.58	20.42	22.12	2924.13
382.48–383.28	A19	2.84	63.09	19.95	14.12	2115.35
390.95–394.13	A20	2.94	48.26	25.03	23.77	3501.01
396.12–398.54	A21	3.74	37.85	27.18	31.22	4351.56
399.66–428.26	A22	2.77	51.66	21.27	24.30	3203.60
390.95–428.26	A23	2.66	53.58	20.58	23.18	3045.16
448.76–450.98	A24	3.44	30.99	28.49	37.08	5036.16
Average		3.82	49.97	23.12	23.10	3203.97

Table 4 Proximate analysis of BH2 (*VM* volatile matter, *GCV* gross calorific value)

Depth (m)	Samples	Moisture (%)	Ash (%)	VM (%)	Fixed carbon (%)	GCV (kcal/kg)
8.40–9.22	B1	7.02	38.02	26.12	28.85	3890.65
59.28–63.40	B2	4.37	54.50	20.07	21.06	2704.77
77.98–80.44	B3	4.80	60.21	17.51	17.48	2133.37
82.32–83.39	B4	5.98	49.57	21.14	23.31	2911.53
88.05–89.12	B5	4.87	54.90	20.03	20.21	2579.48
101.09–103.13	B6	3.98	64.14	17.28	14.60	1852.42
104.61–106.81	B7	4.98	55.28	21.41	18.33	2527.12
128.64–130.58	B8	4.83	50.44	22.02	22.72	3018.70
176.79–177.69	B9	5.77	38.25	25.94	30.04	3997.35
188.32–189.33	B10	4.54	47.77	24.61	23.09	3304.92
199.66–202.18	B11	3.74	58.26	20.65	17.35	2432.03
238.00–267.64	B12	4.94	41.41	26.51	27.13	3830.30
279.05–281.20	B13	3.86	49.89	28.65	17.60	3198.34
285.24–291.33	B14	4.64	44.33	24.97	26.07	3622.12
332.77–333.84	B15	3.77	50.01	21.81	24.41	3202.36
342.05–381.29	B16	2.99	53.35	20.89	22.77	3048.03
402.17–404.19	B17	3.98	37.95	23.24	34.84	4301.03
Average		4.65	48.28	22.83	24.24	3243.64

Table 5 Summary of average values obtained for proximate analysis of four boreholes (*VM* volatile matter, *GCV* gross calorific value)

Borehole name	Depth (m)	Samples	Moisture (%)	Ash (%)	VM (%)	Fixed carbon (%)	GCV (kcal/Kg)
BH1	19.78–450.98	24	3.82	49.97	23.12	23.10	3204
BH2	8.40–404.19	17	4.65	48.28	22.83	24.24	3244
BH3	12.58–416.00	20	4.65	48.28	22.83	24.24	3244
BH4	13.80–375.84	24	5.53	50.86	20.46	23.15	2880

Table 6 Major oxide (%) distribution in coal ash of BH1

Samples	SiO_2	Al_2O_3	Fe_2O_3	K_2O	TiO_2	CaO	MgO	Na_2O	P_2O_5	SO_3
A1	60.6	28.9	3.45	1.89	1.49	1.22	0.91	0.11	0.89	0.19
A2	60	25.3	6.59	2.98	1.2	0.74	1.34	0.15	0.53	0.69
A3	63.7	27.3	2.32	2.52	1.26	0.52	1.19	0.15	0.46	0.3
A4	64.9	25.5	2.64	3.14	1.17	0.46	1.35	0.12	0.25	0.18
A5	65.3	24.4	3.26	3.30	1.08	0.38	1.44	0.14	0.15	0.24
A6	63.2	26.7	3.09	3.12	1.24	0.43	1.42	0.14	0.13	0.24
A7	62.8	25.6	5.07	2.44	1.2	0.72	1.23	0.11	0.31	0.29
A8	60.8	28.9	3.79	2.39	1.33	0.53	1.1	0.08	0.33	0.44
A9	63.5	27.7	2.6	2.48	1.36	0.49	1.15	0.11	0.2	0.22
A10	60.3	29.7	3.48	2.32	1.53	0.53	1.26	0.09	0.18	0.29
A11	59.3	31.4	3.07	1.93	1.6	0.57	0.97	0.08	0.4	0.25
A12	59	32	3.97	1.5	1.66	0.4	0.74	0.07	0.23	0.2
A13	55.5	34.6	4.7	0.89	2.01	0.79	0.57	0.06	0.54	0.1
A14	47.3	37.4	11.15	0.75	1.87	0.27	0.62	–	0.1	0.16
A15	49.8	38.9	6.8	0.86	2.13	0.39	0.52	0.07	0.14	0.06
A16	51.1	37.4	7.33	0.83	1.95	0.28	0.53	0.07	0.1	0.07
A17	61.4	30.6	3.8	0.98	1.88	0.28	0.46	0.06	0.11	0.07
A18	56.1	34.5	4.92	0.93	1.96	0.32	0.54	0.06	0.21	0.09
A19	55	28.3	12.48	0.87	1.58	0.34	0.65	–	0.24	0.13
A20	49.5	35.3	10.17	0.81	1.75	0.82	0.62	–	0.52	0.24
A21	50	31.2	13.05	0.89	1.79	0.92	0.75	0.06	0.66	0.16
A22	57.8	32.8	5.01	0.86	1.86	0.49	0.48	0.06	0.28	0.08
A23	54.9	35.5	5.19	0.83	1.84	0.48	0.49	0.09	0.31	0.1
A24	55	39.7	1.08	0.84	2.17	0.27	0.31	0.09	0.08	0.08
Average	57.78	31.2	5.38	1.68	1.62	0.53	0.86	0.09	0.31	0.203

average content of both major and minor elements (Tables 6 and 7) and (Table S-2a, b) was in the decreasing order of $SiO_2 > Al_2O_3 > Fe_2O_3 > TiO_2 > K_2O > MgO > CaO > P_2O_5 > SO_3 > Na_2O$.

Rare-earth elements

The results obtained for rare-earth concentrations of all the 85 coal ash samples are tabulated in Table 8a-d. The concentration of individual REEs (both LREE and HREE), total REEs, average value of REEs, ratio of LREE/HREE, and outlook coefficient data of all samples are included in the same. Noticeable variation in total REE concentration was found within all the analyzed samples from four boreholes (348.86 to 971.06 ppm) with an average value of 510 ppm. Typically, the concentration of REE increased in coal ash samples as we increased the depth of borehole. This could be collectively suggestive of felsic composition in the source region as weathering of felsic rocks can cause enrichments of LREEs in the residue. The four REEs which were predominantly present were Ce (112–353 ppm), La (69–225 ppm), Nd (44–136 ppm), and Y (34–110 ppm) (Table 8a-d). Lu and Tm, which belong to the HREEs, were present in the lowest concentrations (0.5–1.8 ppm) showing their minimal association with the inorganic matter. The distribution pattern of REEs followed the order Ce > La > Nd > Y > Pr > Sc > Sm > Gd > Dy > Er > Yb > Eu > Ho > Tb > Tm > Lu where the most abundant lanthanide was Ce and the least abundant was Lu. The ratio of ∑LREE/∑HREE among different boreholes varied from 2.56 to 5.35 with an

Table 7 Major oxide (%) distribution in coal ash of BH2

Samples	SiO_2	Al_2O_3	Fe_2O_3	K_20	TiO_2	CaO	MgO	Na_2O	P_2O_5	SO_3
B1	61.9	27.4	3.68	2.58	1.22	0.84	1.18	0.13	0.09	0.53
B2	62.8	27.9	2.87	2.41	1.26	0.61	1.09	0.11	0.46	0.19
B3	64.1	26.1	3.03	3.1	1.14	0.39	1.36	0.14	0.09	0.23
B4	58.57	26.3	4.00	2.92	1.24	0.52	1.34	0.11	0.1	0.34
B5	64	28	2.17	2.23	1.44	0.51	0.96	0.12	0.1	0.15
B6	65.1	27	2.13	2.48	1.32	0.37	0.97	0.12	0.09	0.11
B7	58.6	27.6	7.63	2.29	1.26	0.62	1.16	0.14	0.11	0.24
B8	61.2	29.2	3.14	2.37	1.54	0.51	1.24	0.14	0.1	0.23
B9	56.7	33.7	3.47	1.76	1.67	0.67	0.95	0.08	0.29	0.26
B10	59.6	29.7	5.27	1.67	1.78	0.42	0.79	0.1	0.12	0.25
B11	53.2	36.8	5.49	1.4	1.48	0.27	0.72	0.09	0.1	0.15
B12	51.8	38.2	4.73	0.86	1.98	0.79	0.53	0.07	0.49	0.14
B13	41.6	31.2	22.49	0.77	1.65	0.47	1.01	–	0.15	0.22
B14	52.7	34.6	7.93	0.92	2.05	0.38	0.6	–	0.17	0.24
B15	58	30.2	7.14	0.69	1.91	0.48	0.6	–	0.26	0.14
B16	54.9	35.7	4.83	0.82	1.87	0.5	0.48	0.06	0.31	0.08
B17	56	37.9	1.55	0.86	2.42	0.3	0.33	0.06	0.07	0.05
Average	57.7	31.0	5.39	1.77	1.60	0.51	0.90	0.11	0.18	0.21

average value of 3.85, which validated the higher affinity of LREE (around 80%) for the inorganic matter in Samaleswari coal block. The fraction of HREE remained considerably low (20%) for all of them.

REE distribution and their significance

The method of resource assessment originally proposed by Seredin and Dai typically assisted in evaluating the suitability of coal or its by-product as a source for the extraction of REE. The ratio of critical to excessive REEs in the source (Seredin and Dai 2012) gives us the Outlook Coefficient (C_{outl}), which is instrumental toward suitability assessment of a particular area. In compliance with previous literature, the coal ash samples which were examined proved to be a promising source of REEs based on the calculated C_{outl} (Eq. 1) which varied from 0.7 to 1.0 (Lin et al; 2017; Franus et al; 2015)

$$\text{Coutl} = \frac{(Nd + Eu + Tb + Dy + Er + Y)/\sum REE}{(Ce + Ho + Tm + Yb + Lu)/\sum REE}. \quad (1)$$

The PAAS (Post-Archean Australian Shale) normalized plots (Taylor and McLennan 1985) of all the samples from four boreholes are represented in Fig. 2a-d and Table 8. It showed that all the boreholes demonstrated a similar pattern, indicating similarity in depositional conditions that prevailed throughout the period as REE fractionation is independent of diagenesis. Overall, flat REE pattern indicated a mixed source of sedimentation. The $(La/Yb)_N$ ratio was calculated to quantify the fractionation between LREE and HREE (Table 8). The result showed that the ratio varied between 1.52 and 0.74 for BH1, 1.30 and 0.92 for BH-2, 1.25 and 1.44 for BH-3, and 0.94 and 1.17 for BH-4 and most of the $(La/Yb)_N$ is greater than ≥ 1, which indicated that samples were primarily LREE intensified and possibly associated phosphate and carbonate rocks (Wang and Liang., 2015). Most Eu anomalies were found to be lower than 1, varying from 0.8 to 1, except for BH-2, where it varied from 0.49 to 0.52. BH-2, thus, showed significantly negative Eu anomalies as compared to the other three boreholes. To sum it up, slightly negative Eu anomaly (Eu/Eu*) and high LREE/HREE ratio indicates felsic influence in sedimentation (Tobia et al. 2019).

As presented in Tables 9 and 10 and Table S-3a, b for all the coal ashes which were analyzed in this study, the concentration of critical rare-earth elements varied in the range of 100–300 ppm and C_{outl} ranged from 0.7 to 1.0. Coal seams from the Samaleswari coal block could therefore be considered a promising source of REE elements (Seredin and Dai 2012). To ensure that the conclusion drawn from the study is representative of the whole coal ash stockpile, we chose to analyze 17–24 coal samples from each borehole. The REE content of all the samples was grossly similar to data represented previously by Franus et al. (2015). The total REE content of individual boreholes (Tables 9 and 10) varied within the range of 413–663 ppm (BH1), 349–704 ppm (BH2), 385–615 ppm (BH3), and 363–971 ppm (BH4). Roughly, all the coal ash samples demonstrated their respective REE content to be either similar or significantly higher than the world's average (445 ppm) (Kertis and Yudowich 2009). In accordance with literature precedence Dai et al (2016a),

Table 8 La/Yb_N fractionation and Ce and Eu anomalies' distribution in the four boreholes of Samaleswari coal block

Borehole	Sample	La/Yb	Ce anomalies	Eu anomalies
BH-1	A1	1.52	0.54	1.00
	A2	1.26	0.56	0.96
	A3	1.42	0.51	1.07
	A4	1.23	0.58	0.91
	A5	1.24	0.49	1.00
	A6	1.31	0.51	0.97
	A7	1.27	0.51	0.99
	A8	1.30	0.50	0.99
	A9	1.47	0.39	0.88
	A10	1.42	0.70	1.05
	A11	1.35	0.40	1.04
	A12	1.37	0.54	0.88
	A13	1.43	0.59	1.01
	A14	1.27	0.87	0.91
	A15	1.35	0.89	0.90
	A16	1.34	0.90	0.91
	A17	1.44	0.85	0.92
	A18	1.54	0.83	0.89
	A19	1.69	0.85	0.91
	A20	1.37	0.82	0.89
	A21	1.48	0.83	0.90
	A22	1.54	0.89	0.89
	A23	1.48	0.86	0.91
	A24	0.74	0.87	0.90
BH-2	B1	0.92	0.85	0.49
	B2	1.20	0.86	0.51
	B3	1.18	0.85	0.54
	B4	1.20	0.84	0.52
	B5	1.10	0.86	0.55
	B6	1.16	0.87	0.54
	B7	1.22	0.86	0.51
	B8	1.14	0.87	0.55
	B9	1.43	0.83	0.53
	B10	0.99	0.82	0.50
	B11	1.29	0.86	0.48
	B12	1.29	0.85	0.52
	B13	1.20	0.84	0.52
	B14	1.19	0.88	0.56
	B15	1.99	0.81	0.55
	B16	1.42	0.85	0.57
	B17	1.30	0.85	0.52
BH-3	C1	1.25	0.91	0.92
	C2	1.51	0.90	0.92
	C3	1.42	0.92	0.93
	C4	1.35	0.92	0.92
	C5	1.30	0.90	0.91
	C6	1.37	0.90	0.93
	C7	1.34	0.93	0.94
	C8	1.42	0.91	0.91
	C9	1.30	0.90	0.89
	C10	1.47	0.94	0.91
	C11	1.34	0.95	0.90
	C12	1.24	0.95	0.91
	C13	1.64	0.93	0.92
	C14	1.26	0.93	0.94
	C15	1.20	0.93	0.93
	C16	1.20	0.95	0.95
	C17	1.45	0.92	0.97
	C18	1.42	0.90	0.96
	C19	1.21	0.92	0.96
	C20	2.15	0.93	0.86
	C21	1.46	0.92	0.84
	C22	1.39	0.92	0.86
	C23	1.27	1.02	0.87
	C24	1.44	0.93	0.84
BH-4	D1	0.94	0.92	0.85
	D2	1.34	0.90	0.85
	D3	1.37	0.89	0.86
	D4	1.28	0.89	0.75
	D5	1.14	0.92	0.81
	D6	1.25	0.93	0.83
	D7	1.25	0.93	0.82
	D8	1.27	0.92	0.83
	D9	1.46	0.90	0.82
	D10	1.26	0.92	0.80
	D11	1.43	0.95	0.82
	D12	1.48	0.94	0.82
	D13	1.31	0.93	0.86
	D14	1.19	0.95	0.86
	D15	1.85	0.95	0.87
	D16	1.63	0.91	0.87
	D17	1.52	0.93	0.85
	D18	1.60	0.91	0.86
	D19	1.16	0.89	0.85
	D20	1.17	0.95	0.89

Description: Eu_N/Eu_N*: Eu anomalies $((Eu_n)/(Sm_n*Gd_n)^{0.5})$ Ce_N/Ce_N*: Ce anomalies $((Ce_n)/(La_n*Pr_n)^{0.5})$; La/Yb_N: fractionation of normalized Lanthanum and Ytterbium value, PAAS (Post-Archean Australian Shale) REEs' value was used as a reference for normalization

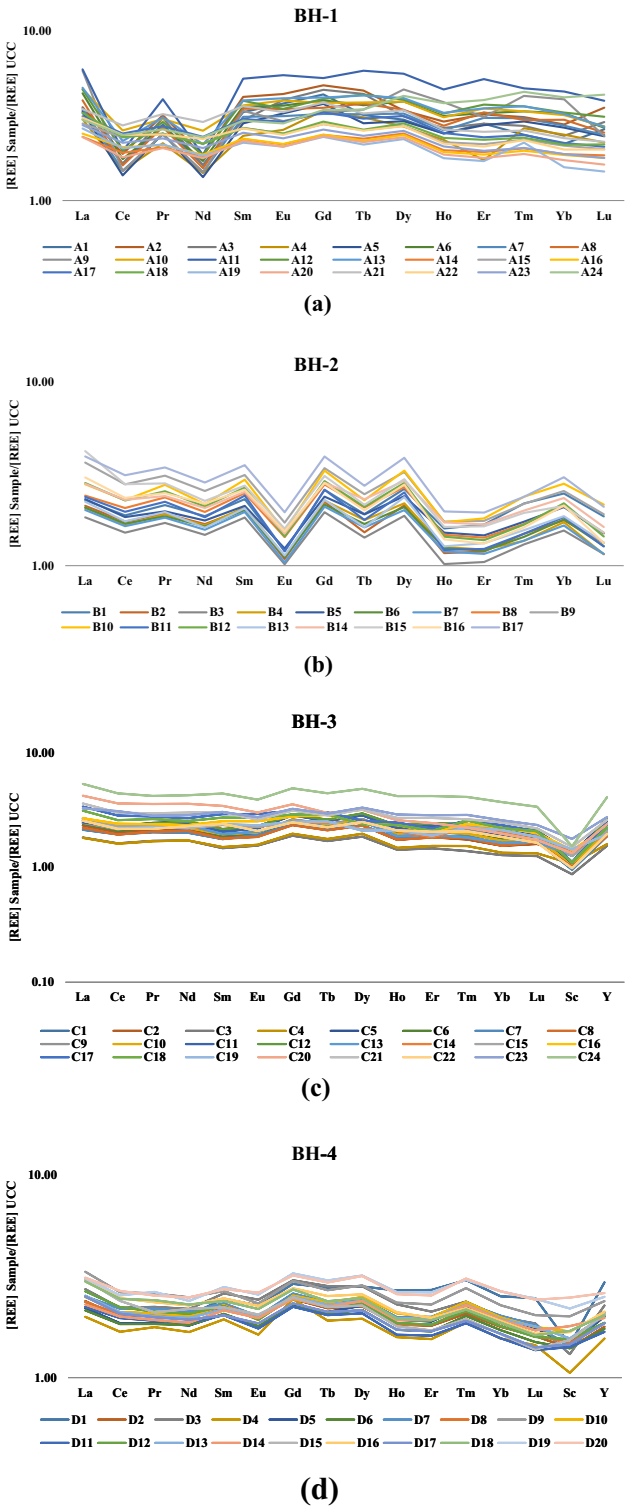

Fig. 2 UCC normalized plots of all the samples from four boreholes

we observed that the concentrations of all REEs except lanthanum (La) and cerium (Ce) are almost similar to world hard coal ash data (Fig. 3). Concentration coefficients (CC) obtained by calculating the ratio of average concentration of REEs in coal ash samples from Samaleswari coal block *vs* average of the corresponding element in world hard coal ash is shown in Fig. 4. It substantiated the fair enrichment of La and Ce ($1 < CC < 2$) along with weak enrichment of Sm ($0.5 < CC < 1$). An overall estimation suggested that the coal samples from the Samaleswari block were profoundly enriched in LREE, but depleted in HREE.

A box and whisker plot is another effective way to graphically display and understand the variation in any set of data obtained from multiple resources. The REE distribution obtained in the coal samples from four boreholes of the Samaleswari block is summarized in Fig. 5. As evident from the plots, BH1 showed a maximum concentration of all REE concentrations except Ce, Nd, Sc, and Y. On the other hand, BH4 exhibited higher values of Ce, Pr, Nd, and Y. BH4 had shown wide range variation between minimum, maximum, and quartiles (Q1, Q2, and Q3) values of Ce (128.74–353.44 ppm). BH2 and BH3 showed the least variation in concentration of REEs among the four boreholes. The concentration of all the HREE and some of LREE (Sm, Eu, La, and Gd) was significantly higher in BH1. Thus, out of the four boreholes, BH1 would be an ideal choice for further investigation on REE extraction.

Agglomerative hierarchical clustering and Pearson correlation

The correlation of REEs with major elemental oxides in the coal ash matrix has been reported previously (Franus et al. 2015; Hood et al. 2017; Wang et al. 2019; Kolker 2017). The occurrence of REE in aluminosilicate glass matrix showing strong positive correlation between Al and Si with REE was consistently found by multiple articles with respect to US coals (Kolker 2017; Stuckman et al. 2018). To delineate the correlation of REEs with the mineralogical framework in coal samples in the present study, multidimensional statistical methods, such as correlation matrix (CM) and agglomerative hierarchical clustering (AHC) analysis, were applied. The agglomerative hierarchical clustering (AHC) analysis has been performed for all the four boreholes under investigation. The dendrograms obtained by the centroid clustering method using SPSS software are presented in Fig. 6a-d. Additionally, the Pearson concentration coefficient of all the samples acquired from four boreholes was analyzed using the chemical data set of rare-earth elements (ppm) and major oxides (%). The data obtained are tabulated in Tables 9 and 10 and Table S-3a, b. A detailed analysis of the primary correlations is as follows.

BH1

The correlation between REE and major oxides of BH1 is presented in Fig. 6a and Table 11. All REEs except Ce, Nd,

Table 9 Comprehensive data of REE (ppm) analysis of the coal samples acquired from BH1 borehole of Samaleswari coal block

Sample	A1	A2	A3	A4	A5	A6	A7	A8	A9	A10	A11	A12	A13	A14	A15	A16	A17	A18	A19	A20	A21	A22	A23	A24
La	124.8	134.8	129.6	114.7	127.0	162.8	133.0	148.0	221.0	172.0	225.3	171.5	175.6	90.2	108.0	94.2	119.3	124.9	101.0	89.9	131.4	117.0	105.7	113.6
Ce	132.0	150.7	131.8	119.8	112.5	140.4	119.8	128.9	119.1	207.0	156.7	156.9	179.4	153.0	188.7	165.1	198.7	189.1	162.6	144.0	221.8	194.7	175.1	194.4
Pr	24.9	28.3	27.3	19.4	22.1	24.4	21.8	24.1	22.0	26.9	35.2	25.8	27.5	18.3	22.1	18.9	24.4	22.0	19.0	18.1	28.7	21.8	20.7	23.4
Nd	51.8	58.5	51.8	46.5	44.0	54.7	47.1	49.6	46.9	82.5	59.4	59.4	68.7	57.3	69.3	59.7	75.9	69.0	58.7	56.9	92.9	73.7	65.2	75.5
Sm	18.6	22.9	16.6	13.5	16.0	20.0	17.4	19.5	18.9	20.4	29.3	21.7	21.8	12.9	15.0	13.0	16.9	15.0	12.3	12.6	20.1	14.9	14.0	16.6
Eu	4.1	4.7	4.3	2.9	3.6	4.0	3.5	3.8	3.2	4.3	6.0	3.8	4.4	2.4	2.7	2.4	3.2	2.7	2.3	2.3	3.7	2.7	2.6	3.1
Gd	19.8	22.4	21.1	15.9	17.5	18.3	15.2	16.5	15.5	17.7	24.8	18.7	19.0	11.4	13.3	11.5	15.5	13.7	11.2	11.3	17.7	13.3	12.3	16.1
Tb	2.5	3.4	3.3	2.4	2.2	2.8	2.5	2.9	2.6	2.9	4.5	3.2	3.2	1.8	2.0	1.7	2.3	2.0	1.6	1.7	2.5	2.0	1.9	2.6
Dy	13.2	14.9	13.8	12.0	12.9	16.9	14.3	15.1	19.9	16.9	24.6	17.3	17.7	10.9	12.1	10.7	13.9	12.5	10.1	10.4	15.0	12.1	11.3	18.2
Ho	2.5	2.9	2.7	2.3	2.5	3.1	2.6	2.8	3.8	3.1	4.5	3.3	3.3	2.0	2.2	1.9	2.5	2.3	1.8	1.9	2.6	2.2	2.1	3.7
Er	8.2	9.3	8.2	5.0	8.1	9.5	8.9	9.6	9.0	10.1	15.1	10.7	10.1	5.6	6.2	5.4	6.8	6.6	5.0	5.2	7.4	6.0	5.7	11.3
Tm	1.0	1.2	1.1	1.1	1.2	1.3	1.2	1.2	1.7	1.3	1.8	1.4	1.4	0.8	0.9	0.8	1.0	0.9	0.9	0.8	1.0	0.9	0.8	1.7
Yb	6.0	7.9	6.7	6.8	7.5	9.1	7.7	8.4	11.1	8.9	12.3	9.2	9.1	5.3	5.9	5.2	6.1	6.0	4.4	4.8	6.5	5.6	5.3	11.4
Lu	1.1	1.5	1.2	0.9	1.0	1.2	1.0	1.1	1.0	1.2	1.7	1.3	1.2	0.8	0.9	0.8	0.9	0.9	0.6	0.7	1.0	0.9	0.8	1.8
Sc	21.0	17.7	18.7	14.1	15.1	16.4	13.1	16.0	16.9	19.3	16.5	13.5	13.2	19.5	16.1	18.1	17.1	20.1	17.5	12.7	18.9	12.2	14.6	23.3
Y	39.3	49.2	39.8	36.5	33.6	43.2	39.4	38.8	36.4	68.9	44.9	50.4	44.8	45.9	51.5	45.3	57.4	58.5	42.0	43.3	60.5	53.2	47.6	98.6
∑REE	470.8	530.4	478.0	413.8	426.7	528.2	448.6	486.3	549.1	663.4	662.4	568.1	600.3	438.0	517.0	454.6	562.1	546.3	451.1	416.4	631.9	533.1	485.6	615.3
LREEs	376.1	422.3	382.5	332.6	342.7	424.7	357.8	390.5	446.7	530.8	536.6	457.8	496.3	345.4	419.2	364.7	454.0	436.3	367.2	335.0	516.4	438.1	395.7	442.6
HREEs	94.7	108.0	95.5	81.1	84.0	103.5	90.7	95.7	102.3	132.5	125.8	110.3	103.9	92.5	97.7	89.8	108.0	109.9	83.9	81.3	115.4	95.0	89.9	172.7
Critical	119.0	140.0	121.2	105.3	104.3	131.1	115.7	119.8	118.1	185.6	154.4	144.8	148.8	123.8	143.9	125.2	159.6	151.4	119.8	119.7	181.9	149.8	134.3	209.4
Excessive	142.6	164.3	143.5	131.0	124.7	155.2	132.4	142.3	136.7	221.6	177.0	172.2	194.3	161.9	198.6	173.8	209.2	199.2	170.3	152.1	233.0	204.2	184.0	213.1
Uncritical	209.1	226.1	213.3	177.5	197.7	241.9	200.5	224.2	294.3	256.2	331.0	251.1	257.1	152.3	174.5	155.6	193.4	195.7	161.0	144.6	217.0	179.2	167.3	192.9
Coutl	0.8	0.9	0.8	0.8	0.8	0.8	0.9	0.8	0.9	0.8	0.9	0.8	0.8	0.8	0.7	0.7	0.8	0.8	0.7	0.8	0.8	0.7	0.7	1.0
LREE/ HREE	4.0	3.9	4.0	4.1	4.1	4.1	3.9	4.1	4.4	4.0	4.3	4.2	4.8	3.7	4.3	4.1	4.2	4.0	4.4	4.1	4.5	4.6	4.4	2.6

Table 10 Comprehensive data of REE (ppm) analysis of the coal samples acquired from BH2 borehole of Samaleswari coal block

Sample	B1	B2	B3	B4	B5	B6	B7	B8	B9	B10	B11	B12	B13	B14	B15	B16	B17
La	86.42	80.53	69.63	78.52	87.52	78.67	76.42	91.51	138.4	105.6	89.99	107.2	84.72	105.9	159.9	114.9	150
Ce	150.4	139.2	121	133.3	147.2	135.7	131.4	164.9	221.9	181.9	157.3	181.3	139.6	182.5	222.1	187.2	249
Pr	19.01	17.08	15.21	16.94	17.58	16.52	16.24	20.94	27.52	24.54	19.83	22.63	17.43	21.32	24.98	22.11	30.5
Nd	59.52	53.88	47.09	53.08	56.4	52.32	50.22	62.74	81.6	69.23	58.75	67.16	51.5	65.94	72.05	69.73	90.8
Sm	12.9	11.41	10.24	11.62	11.85	11.24	10.98	13.91	17.47	16.47	13.48	14.93	11.51	14.13	15.28	14.53	19.8
Eu	1.32	1.2	1.12	1.24	1.36	1.22	1.15	1.57	1.89	1.7	1.32	1.59	1.25	1.65	1.75	1.69	2.15
Gd	12.16	10.47	9.19	10.63	11.17	10.11	9.85	13.01	15.96	15.48	12.18	13.57	10.73	13.31	14.48	13.26	18.5
Tb	1.47	1.17	1.09	1.36	1.46	1.3	1.25	1.6	1.89	1.75	1.37	1.61	1.25	1.77	1.65	1.54	2.1
Dy	11.53	9.38	8.22	9.61	10.52	9.17	8.84	11.79	14.25	14.48	11.02	12.41	10.39	12.76	13.02	12.17	17
Ho	1.6	1.17	1.02	1.26	1.51	1.25	1.2	1.47	1.74	1.73	1.22	1.44	1.27	1.72	1.63	1.39	1.97
Er	4.86	3.46	3.03	3.55	4.24	3.5	3.36	4.12	5.09	5.25	3.58	3.99	3.85	4.87	4.75	3.83	5.64
Tm	0.87	0.6	0.52	0.55	0.69	0.57	0.55	0.67	0.87	0.95	0.6	0.67	0.62	0.8	0.78	0.65	0.95
Yb	6.92	4.95	4.35	4.83	5.84	5	4.63	5.92	7.14	7.83	5.15	6.12	5.21	6.54	5.92	5.96	8.49
Lu	0.8	0.57	0.5	0.5	0.64	0.55	0.5	0.65	0.82	0.93	0.55	0.62	0.57	0.7	0.65	0.57	0.9
Sc	22.46	17.33	18.44	17.07	20.96	19.73	18.69	26.87	24.04	23.09	22.04	23.62	22.09	27.34	29.77	24.81	34.4
Y	62.24	43.97	38.18	44.62	54.22	42.78	39.49	49.68	61.97	56.28	42.25	48.76	43.31	55.96	58.3	56.04	72.6
RE	454.4	396.4	348.9	388.7	433.1	389.6	374.7	471.3	622.5	527.1	440.6	507.5	405.3	517.2	627	530.3	704
LREEs	341.7	313.8	273.5	305.3	333	305.8	296.2	368.6	504.7	414.8	352.8	408.3	316.7	404.8	510.5	423.4	560
HREEs	112.7	82.6	75.4	83.3	100.1	83.8	78.5	102.8	117.8	112.3	87.8	99.2	88.6	112.5	116.5	106.9	144
Critical	140.9	113.1	98.7	113.5	128.2	110.3	104.3	131.5	166.7	148.7	118.3	135.5	111.5	142.9	151.5	145	190
Excessive	160.5	146.5	127.4	140.4	155.8	143	138.3	173.6	232.4	193.3	164.8	190.1	147.3	192.3	231.1	195.7	261
Uncritical	152.9	136.8	122.7	134.8	149.1	136.3	132.2	166.2	223.4	185.1	157.5	181.9	146.5	182	244.4	189.6	253
C_{OUT}	0.88	0.77	0.78	0.81	0.82	0.77	0.75	0.76	0.72	0.77	0.72	0.71	0.76	0.74	0.66	0.74	0.73
LREE/HREE	3.03	3.8	3.63	3.66	3.33	3.65	3.77	3.59	4.28	3.69	4.02	4.11	3.58	3.6	4.38	3.96	3.88

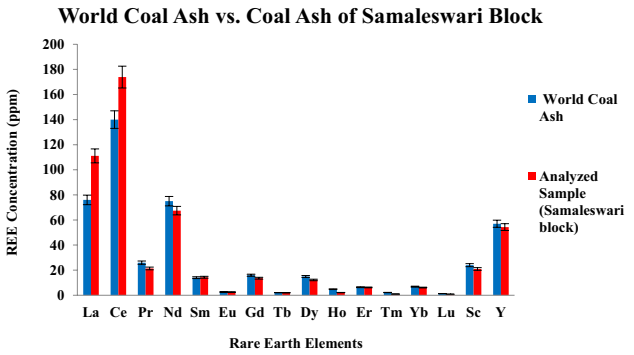

Fig. 3 Comparison of REE content between World Coal Ash and Coal Ash of Samaleswari Coal Block

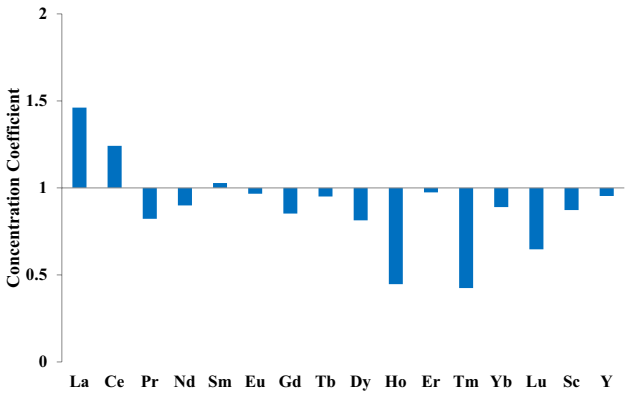

Fig. 4 Concentration Coefficient (CC, average concentration of element in coal ash samples investigated vs. average of corresponding element in world hard coal ash). World hard coal ash data were taken from Wang et al. (2019)

Y, and Sc showed positive correlation and affinity with the major oxides, such as SiO_2, K_2O, MgO, Na_2O, and SO_3, but negative correlation with Al_2O_3 and TiO_2. Nevertheless, Ce, Sc, Nd, and Y (Sc being the strongest) demonstrated a strong affinity and positive concentration coefficient with Al_2O_3 and TiO_2 ($r = 0.5$–0.76) and a weak association with other oxides. The correlation between all the major oxides (SiO_2, K_2O, Na_2O, and MgO) was noticeably high ($0.7 < r < 0.97$). Calcium and phosphorus showed positive correlation with each other ($r = 0.94$), supporting the abundance of apatite in the coal samples of BH1. The positive correlation of La, Ce, and Nd with TiO_2 ($r = 0.76$) is suggestive of melting of monazite [(Ce, La, Nd, Th)PO_4] or REE-bearing titanium mineral (titanate) resulting in dispersion of REEs in glass phase. Mafic–felsic igneous and metamorphic rocks commonly possess titanate mineral which can preserve multivalent trace elements via substitution.

BH2

In BH2, all REEs demonstrated positive correlation with only two oxides—TiO_2 and Al_2O_3 with concentration coefficients ranging between ($0.6 < r < 0.9$) and ($0.3 < r < 0.7$), respectively (Fig. 6 and Table 12). The co-occurrence of REEs with clay minerals (kaolinite and illite) and titanate is well documented (Rautenbach 2021). Fe-containing aluminosilicate mineral phase showed a positive correlation with all the REEs, although weaker for some. Ca, Fe-enriched aluminosilicate glasses are well known to be enriched with REEs compared to pure aluminosilicates (Kolker et al. 2017). Of note, Al-substituted apatite ($Ca_5(PO_4)_3$) showed good correlation with all the REEs.

BH3 and BH4

Hierarchical clustering and coefficient correlation enumerating the results obtained for borehole BH3 (Table S-4a and Fig. 6c) and BH4 (Table S-4b and Fig. 6c) demonstrated a similar pattern with respect to the association of REE and major oxides. The result clearly showed that both LREEs and HREEs were only associated with TiO_2 ($0.6 < r < 0.8$), indicating a strong correlation with titanate mineral. Smaller correlation coefficients of HREEs in particular with terrigenous elements (SiO_2, Al_2O_3, Fe_2O_3) confirm their comparatively stronger association with the organic matter in coal.

Mineralogical characterization

The mineralogical composition of coal ash is dependent on the geochemistry and properties of feed coal and also on ash temperature. Coal ash is highly enriched with REEs; however, on contrary, REE-bearing minerals are less common in coal ash than coal. Such contradictions not only make the analysis of REEs with coal ash matrix highly complicated, but it also leads to a range of possible alternatives to trace phase retention. Thus, comparison and cross-validation of the results obtained from various analytical methodologies, such as XRD, XRF, and EPMA (shown in subsequent section), were desirable to provide an overall scenario of REE association in the selected coal block. Profiling of the major oxides present in all the coal ash samples is presented in Tables 6 and 7 and Table S-2a, b. Typically, Indian coal ashes are characterized by relatively higher concentrations of SiO_2 and Al_2O_3 followed by contents of Fe_2O_3, which tallies well with our results. These elements are mainly brought in by quartz, clay minerals, and pyrites (Zhao et al. 2013).

Owing to its geological origin, Indian coal seams are sandwiched in between sandstone and shale deposited in the form of rhythmic layers (Singh et al. 2013), resulting in higher percentage of quartz in Indian coals (Bandopadhyay and Chatterjee 2006; Mukherjee and Srivastava 2006). Silica (SiO_2), which is present in ~ 60% concentration in our

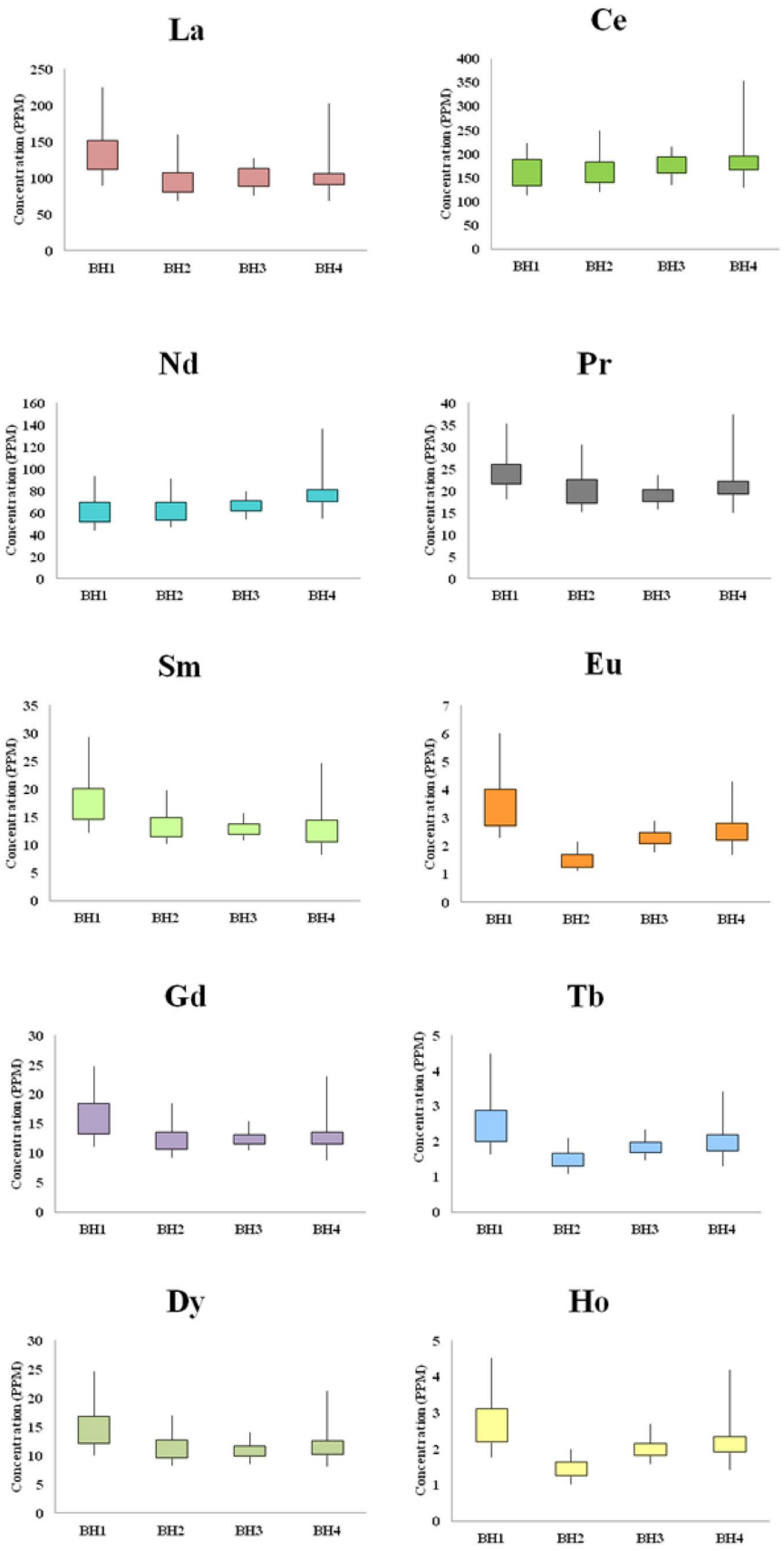

Fig. 5 Box-and-whisker plots of rare-earth element (ppm) in coal ash samples of BH1, BH2, BH4, and BH3. The box expressed Q1 (lower side of the box)—25% quartile, Q3 (upper side of the box)—75% quartile

Fig. 5 (continued)

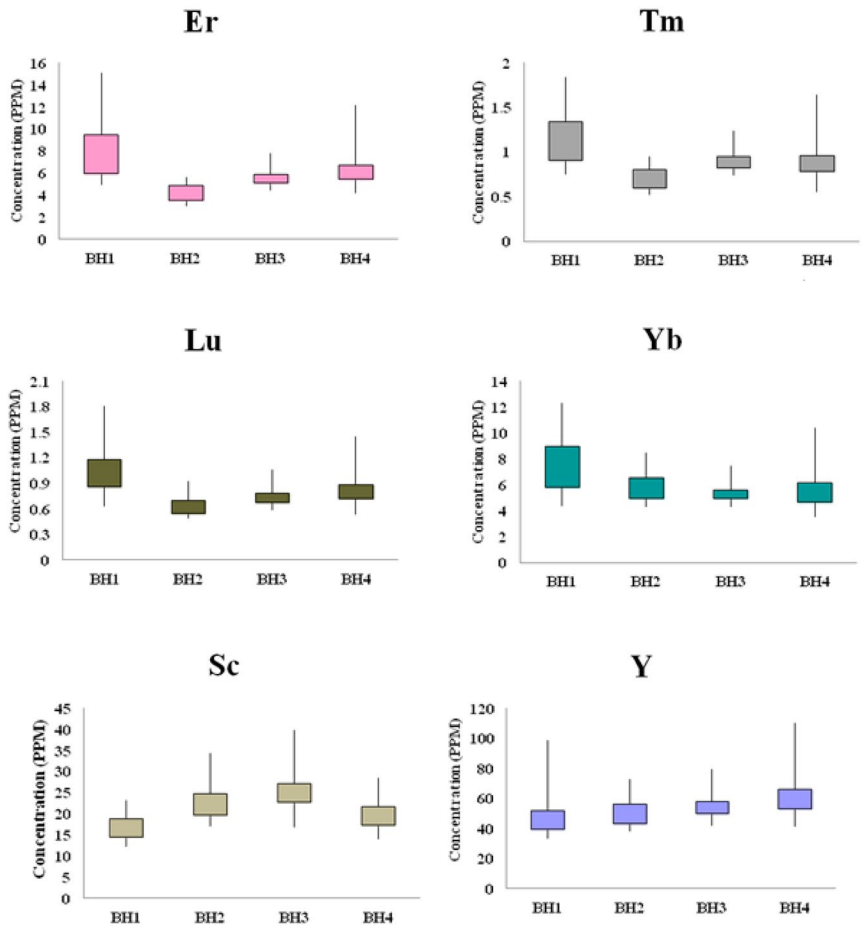

coal ash samples (Tables 6 and 7a-d), is primarily present as quartz rather than clay mineral. XRD studies revealed the presence of higher proportions of quartz, and smaller proportions of anatase (TiO_2), apatite (($Ca_5(PO_4)_3$), and hematite (Fe_2O_3) (Fig. 7a-d) in these samples. XRF analysis demonstrated that 23–41% of the coal ash composition comprises Al_2O_3 (Tables 6 and 7); nonetheless, their corresponding peaks were absent in X-ray diffractograms. It was concluded to be due to conversion of kaolinite ($(Al_2Si_2O_5(OH)_4)$) and illite ($K_{1.5}Al_4(Si_{6.5}Al_{1.5})\ O_{20}(OH)_4$) to metakaolinite and mullite at elevated temperatures (Varga 2007; Rautenbach 2021).

EPMA study

Minerals and poorly crystalline mineroloids are highly probable sites for rare-earth enrichment. Although delineation of exact association of REEs with coal ash minerals is an arduous task, some possible associations with major oxides can be detected to portray the variations in affinity. According to literature precedence, the majority of REEs were either dispersed throughout the glass phase (AlSiK matrix) or as trace phases partitioning into the glass phase or as independent particles outside the glass matrix (Hower et al. 2013; Hood et al. 2017; Kolker et al. 2017). The EPMA point analysis results of some of the selected coal ash samples (Table 13, Figs. 8, 9, 10 and 11), supported by their correlation pattern (Fig. 7a-d), demonstrated the possible presence of REE-bearing titanium mineral (e.g., titanite [$CaTiSiO_5$] (King et al. 2012)) in these boreholes. It was thus speculated that the REEs were dispersed in the glass phase as Ti co-existed with Si and to a large extent with Ca in all the coal ash samples. Interestingly, in BH4, prominent correlation was observed between Ti and Ce which has literature precedence (King et al. 2012). The co-localization of Ce, La, and Nd, but not Sm, in the aluminosilicate matrix was considered as direct evidence of dispersion of LREE enriched monazite into the glass phase of our chosen coal block, supporting previous hypothesis (Mohanty et al. 2003; Stuckman 2018; Hood et al. 2017; Kolker et al. 2017). Incorporation of Fe into the glass phase resulting in fine intergrowths of Fe-oxides during coal combustion has literature precedence (Yang et al. 2014). The proportions of Fe-oxides were highly variable throughout the four boreholes; however, they were found to be closely associated with REE-bearing glass phase

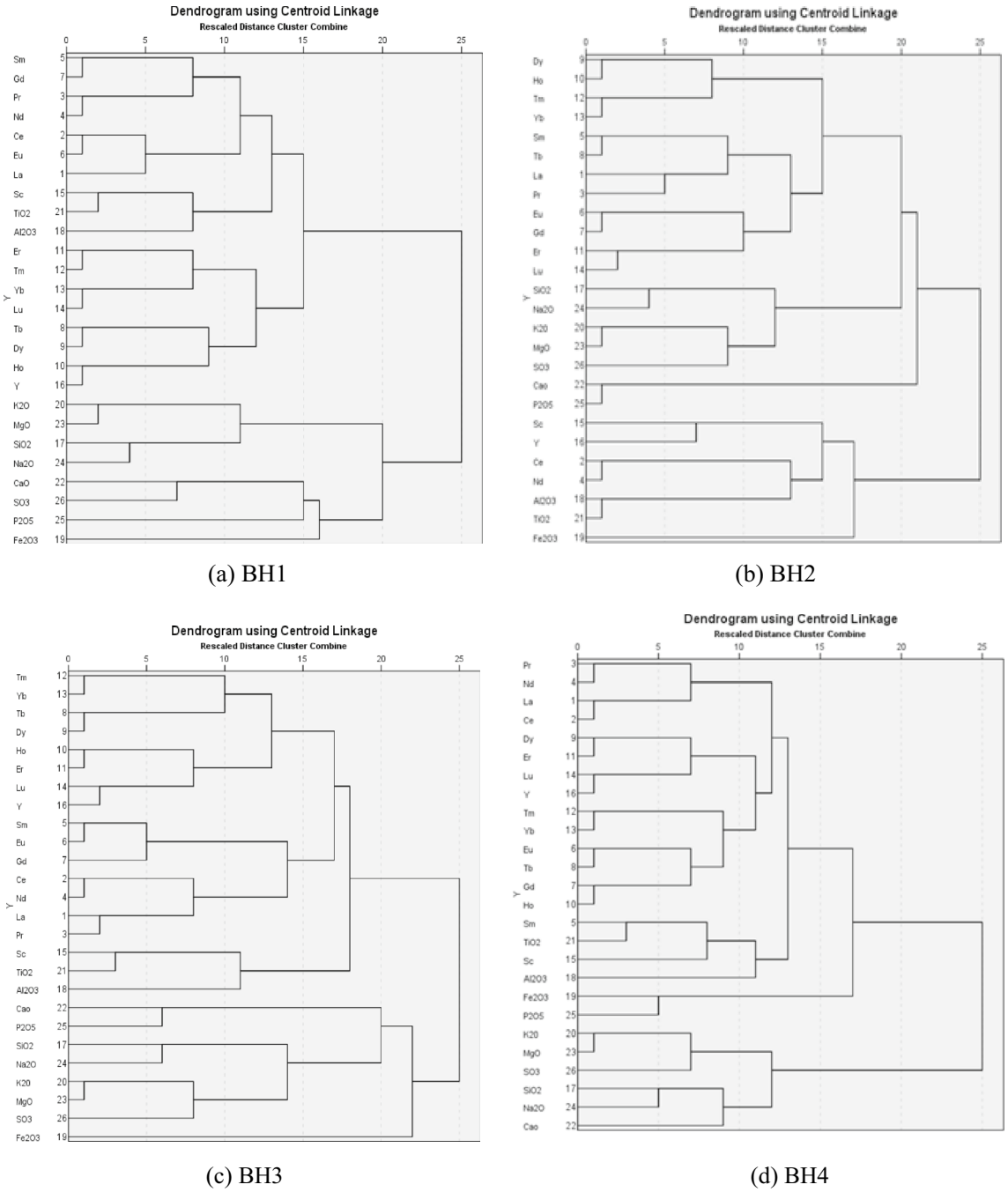

Fig. 6 Hierarchical cluster of analytical data of rare-earth elements and major elements of coal ash samples

particularly in BH1 and BH2, supported by both EPMA (Table 13) and XRF results (Tables 6 and 7).

Further, a qualitative analysis of REE enrichment for two boreholes, BH1 and BH4, is shown in Figs. 12 and 13, respectively. The results obtained by SEM-EDAX analysis were in fair agreement with the conclusions drawn from EPMA and XRD analysis. It reinstated that REEs in the chosen boreholes were present in an encapsulated manner in the Fe–Al–Si matrix of coal ash samples.

Provenance and paleodepositional settings

The oxides' form of inorganic constituents provides useful information about the inorganic matter source (provenance), paleoclimate, paleotectonic, and paleodepositional setting of the region (Ward 2002; Dai et al. 2016b; Zhao et al. 2017). The high concentrations of SiO_2 and Al_2O_3 suggest the existence of a substantial amount of aluminosilicate minerals in Samaleswari coals (Tables 6 and 7 and Tables S4a,b). For

Table 11 Correlation coefficient between rare-earth elements and major oxides (BH1)

	La	Ce	Pr	Nd	Sm	Eu	Gd	Tb	Dy	Ho	Er	Tm	Yb	Lu	Sc
La	1														
Ce	− 0.14	1													
Pr	0.69	0.20	1												
Nd	− 0.08	0.98	0.27	1											
Sm	0.83	0.03	0.93	0.10	1										
Eu	0.74	− 0.11	0.93	− 0.03	0.93	1									
Gd	0.66	− 0.16	0.90	− 0.07	0.87	0.96	1								
Tb	0.79	− 0.11	0.90	− 0.05	0.93	0.95	0.93	1							
Dy	0.91	0.01	0.78	0.07	0.88	0.78	0.72	0.86	1						
Ho	0.87	− 0.03	0.74	0.03	0.84	0.76	0.73	0.85	0.99	1					
Er	0.80	− 0.04	0.81	0.01	0.90	0.86	0.79	0.89	0.93	0.93	1				
Tm	0.82	− 0.10	0.63	− 0.05	0.76	0.69	0.66	0.79	0.94	0.97	0.91	1			
Yb	0.83	− 0.12	0.62	− 0.06	0.76	0.69	0.65	0.79	0.95	0.97	0.91	0.99	1		
Lu	0.54	− 0.02	0.72	0.03	0.74	0.76	0.79	0.83	0.78	0.84	0.88	0.84	0.83	1	
Sc	− 0.09	0.27	0.15	0.28	0.02	0.08	0.13	0.03	0.10	0.16	0.14	0.12	0.11	0.32	1
Y	− 0.11	0.74	0.15	0.74	0.04	− 0.05	− 0.04	0.02	0.20	0.25	0.23	0.26	0.24	0.41	0.53
SiO_2	0.48	− 0.54	0.27	− 0.49	0.33	0.47	0.53	0.45	0.35	0.38	0.36	0.44	0.43	0.35	− 0.15
Al_2O_3	− 0.33	0.58	− 0.22	0.49	− 0.27	− 0.41	− 0.46	− 0.32	− 0.14	− 0.13	− 0.15	− 0.19	− 0.16	− 0.10	0.20
Fe_2O_3	− 0.47	0.28	− 0.29	0.27	− 0.34	− 0.43	− 0.48	− 0.48	− 0.50	− 0.57	− 0.53	− 0.58	− 0.61	− 0.57	− 0.02
K_2O	0.41	− 0.68	0.24	− 0.60	0.34	0.50	0.56	0.45	0.29	0.32	0.33	0.38	0.40	0.34	− 0.10
TiO_2	− 0.29	0.76	− 0.12	0.67	− 0.22	− 0.38	− 0.43	− 0.31	− 0.11	− 0.12	− 0.16	− 0.18	− 0.19	− 0.13	0.20
CaO	0.15	− 0.12	0.35	− 0.01	0.35	0.39	0.40	0.24	0.10	0.07	0.15	0.00	− 0.01	0.10	− 0.08
MgO	0.41	− 0.65	0.25	− 0.55	0.35	0.50	0.52	0.42	0.25	0.26	0.29	0.31	0.33	0.24	− 0.12
Na_2O	0.34	− 0.41	0.36	− 0.35	0.36	0.52	0.62	0.47	0.32	0.38	0.37	0.40	0.42	0.50	0.06
P_2O_5	0.09	− 0.09	0.40	0.01	0.33	0.40	0.44	0.27	0.05	0.03	0.11	− 0.06	− 0.09	0.12	− 0.01
SO_3	0.27	− 0.44	0.36	− 0.36	0.45	0.52	0.53	0.50	0.22	0.24	0.35	0.24	0.26	0.39	− 0.03
$SiO_2+Al_2O_3+Fe_2O_3$	− 0.42	0.57	− 0.43	0.45	− 0.49	− 0.64	− 0.70	− 0.54	− 0.32	− 0.34	− 0.39	− 0.35	− 0.37	− 0.41	0.04
$Al_2O_3+P_2O_5+CaO$	− 0.33	0.58	− 0.19	0.50	− 0.25	− 0.38	− 0.43	− 0.30	− 0.13	− 0.13	− 0.14	− 0.19	− 0.17	− 0.10	0.20
$MgO+Al_2O_3+SiO_2$	0.38	− 0.14	0.17	− 0.17	0.21	0.26	0.29	0.35	0.44	0.50	0.44	0.52	0.54	0.48	0.03
$SiO_2+Al_2O_3+K_2O$	0.42	− 0.25	0.20	− 0.27	0.25	0.33	0.36	0.40	0.45	0.52	0.46	0.54	0.57	0.51	0.01

	Y	SiO_2	Al_2O_3	Fe_2O_3	K_2O	TiO_2	CaO	MgO	Na_2O	P_2O_5	SO_3	$SiO_2+Al_2O_3+Fe_2O_3$	$Al_2O_3+P_2O_5+CaO$	$MgO+Al_2O_3+SiO_2$	$SiO_2+Al_2O_3+K_2O$
La															
Ce															
Pr															
Nd															
Sm															
Eu															

Table 11 (continued)

	Y	SiO_2	Al_2O_3	Fe_2O_3	K_2O	TiO_2	CaO	MgO	Na_2O	P_2O_5	SO_3	$SiO_2+Al_2O_3+Fe_2O_3$	$Al_2O_3+P_2O_5+CaO$	$MgO+Al_2O_3+SiO_2$	$SiO_2+Al_2O_3+K_2O$
Gd															
Tb															
Dy															
Ho															
Er															
Tm															
Yb															
Lu															
Sc															
Y	1														
SiO_2	− 0.31	1													
Al_2O_3	0.53	− 0.82	1												
Fe_2O_3	− 0.09	− 0.74	0.24	1											
K_2O	− 0.42	0.83	− 0.85	− 0.51	1										
TiO_2	0.60	− 0.77	0.94	0.27	− 0.92	1									
CaO	− 0.23	0.04	− 0.26	0.12	0.13	− 0.23	1								
MgO	− 0.48	0.73	− 0.86	− 0.33	0.97	− 0.94	0.21	1							
Na_2O	− 0.15	0.76	− 0.59	− 0.69	0.81	− 0.64	0.14	0.70	1						
P_2O_5	− 0.24	− 0.01	− 0.22	0.17	0.04	− 0.17	0.94	0.11	0.09	1					
SO_3	− 0.26	0.39	− 0.60	− 0.09	0.67	− 0.69	0.32	0.70	0.47	0.31	1				
$SiO_2+Al_2O_3+Fe_2O_3$	0.39	− 0.68	0.81	0.36	− 0.91	0.86	− 0.50	− 0.92	− 0.76	− 0.42	− 0.78	1			
$Al_2O_3+P_2O_5+CaO$	0.52	− 0.83	1.00	0.26	− 0.85	0.94	− 0.17	− 0.86	− 0.59	− 0.13	− 0.58	0.78	1		
$MgO+Al_2O_3+SiO_2$	0.19	0.60	− 0.03	− 0.96	0.29	− 0.05	− 0.30	0.10	0.52	− 0.33	− 0.13	− 0.09	− 0.07	1	
$SiO_2+Al_2O_3+K_2O$	0.11	0.70	− 0.17	− 0.99	0.44	− 0.20	− 0.26	0.25	0.62	− 0.30	− 0.01	− 0.23	− 0.20	0.99	1

Table 12 Correlation coefficient between rare-earth elements and major oxides (BH2)

	La	Ce	Pr	Nd	Sm	Eu	Gd	Tb	Dy	Ho	Er	Tm	Yb	Lu	Sc
La	1														
Ce	0.97	1													
Pr	0.92	0.98	1												
Nd	0.91	0.98	0.99	1											
Sm	0.87	0.95	0.99	0.98	1										
Eu	0.91	0.97	0.98	0.98	0.97	1									
Gd	0.87	0.95	0.99	0.98	1.00	0.97	1								
Tb	0.82	0.92	0.94	0.95	0.95	0.96	0.96	1							
Dy	0.85	0.93	0.97	0.96	0.98	0.96	0.99	0.96	1						
Ho	0.77	0.85	0.86	0.87	0.87	0.89	0.90	0.95	0.93	1					
Er	0.74	0.81	0.84	0.84	0.85	0.84	0.88	0.91	0.91	0.98	1				
Tm	0.68	0.76	0.81	0.80	0.83	0.79	0.86	0.85	0.89	0.94	0.98	1			
Yb	0.68	0.80	0.86	0.86	0.89	0.86	0.91	0.91	0.94	0.95	0.96	0.97	1		
Lu	0.59	0.70	0.78	0.76	0.81	0.75	0.84	0.82	0.86	0.90	0.95	0.98	0.97	1	
Sc	0.84	0.88	0.84	0.84	0.82	0.88	0.84	0.84	0.85	0.81	0.76	0.69	0.73	0.62	1
Y	0.78	0.84	0.84	0.88	0.84	0.86	0.87	0.88	0.88	0.94	0.93	0.90	0.92	0.85	0.78
SiO_2	− 0.23	− 0.24	− 0.23	− 0.19	− 0.22	− 0.21	− 0.22	− 0.18	− 0.27	− 0.12	− 0.12	− 0.06	− 0.11	0.00	− 0.28
Al_2O_3	0.58	0.67	0.67	0.68	0.69	0.66	0.66	0.61	0.66	0.45	0.39	0.36	0.49	0.31	0.63
Fe_2O_3	− 0.08	− 0.15	− 0.17	− 0.24	− 0.20	− 0.19	− 0.18	− 0.22	− 0.12	− 0.15	− 0.10	− 0.13	− 0.19	− 0.18	− 0.02
K_2O	− 0.69	− 0.68	− 0.62	− 0.60	− 0.59	− 0.63	− 0.60	− 0.55	− 0.63	− 0.49	− 0.46	− 0.40	− 0.44	− 0.30	− 0.69
TiO_2	0.80	0.86	0.83	0.83	0.83	0.88	0.84	0.83	0.86	0.75	0.69	0.62	0.71	0.56	0.87
CaO	− 0.07	− 0.09	− 0.08	− 0.06	− 0.09	− 0.12	− 0.09	− 0.07	− 0.10	0.00	0.02	0.07	0.02	0.05	− 0.25
MgO	− 0.73	− 0.76	− 0.71	− 0.72	− 0.71	− 0.73	− 0.70	− 0.66	− 0.72	− 0.59	− 0.52	− 0.48	− 0.57	− 0.41	− 0.72
Na_2O	− 0.60	− 0.53	− 0.44	− 0.41	− 0.38	− 0.46	− 0.41	− 0.39	− 0.45	− 0.39	− 0.39	− 0.30	− 0.27	− 0.17	− 0.55
P_2O_5	0.25	0.21	0.17	0.18	0.13	0.15	0.11	0.03	0.07	− 0.05	− 0.08	− 0.05	− 0.03	− 0.08	− 0.03
SO_3	− 0.36	− 0.36	− 0.29	− 0.30	− 0.27	− 0.34	− 0.24	− 0.18	− 0.21	− 0.03	0.07	0.13	0.00	0.12	− 0.35
$SiO_2+Al_2O_3+Fe_2O_3$	0.45	0.46	0.41	0.39	0.39	0.42	0.39	0.32	0.42	0.31	0.31	0.32	0.33	0.27	0.56
$Al_2O_3+P_2O_5+CaO$	0.58	0.67	0.67	0.68	0.68	0.66	0.65	0.61	0.65	0.45	0.39	0.35	0.49	0.31	0.61

	Y	SiO_2	Al_2O_3	Fe_2O_3	K_2O	TiO_2	CaO	MgO	Na_2O	P_2O_5	SO_3	$SiO_2+Al_2O_3+Fe_2O_3$	$Al_2O_3+P_2O_5+CaO$
La													
Ce													
Pr													
Nd													
Sm													
Eu													

Table 12 (continued)

	Y	SiO_2	Al_2O_3	Fe_2O_3	K_2O	TiO_2	CaO	MgO	Na_2O	P_2O_5	SO_3	$SiO_2+Al_2O_3+Fe_2O_3$	$Al_2O_3+P_2O_5+CaO$
Gd													
Tb													
Dy													
Ho													
Er													
Tm													
Yb													
Lu													
Sc													
Y	1												
SiO_2	− 0.03	1											
Al_2O_3	0.43	− 0.62	1										
Fe_2O_3	− 0.25	− 0.80	0.07	1									
K_2O	− 0.43	0.74	− 0.81	− 0.44	1								
TiO_2	0.68	− 0.50	0.80	0.10	− 0.86	1							
CaO	0.08	0.07	− 0.15	− 0.05	0.17	− 0.24	1						
MgO	− 0.57	0.42	− 0.85	0.00	0.88	− 0.89	0.26	1					
Na_2O	− 0.33	0.74	− 0.55	− 0.59	0.86	− 0.70	0.22	0.65	1				
P_2O_5	0.00	− 0.20	0.35	− 0.01	− 0.34	0.21	0.49	− 0.31	− 0.28	1			
SO_3	− 0.01	0.14	− 0.49	0.07	0.50	− 0.51	0.54	0.63	0.30	− 0.24	1		
$SiO_2+Al_2O_3+Fe_2O_3$	0.27	− 0.38	0.61	0.26	− 0.75	0.60	− 0.30	− 0.73	− 0.52	0.17	− 0.58	1	
$Al_2O_3+P_2O_5+CaO$	0.43	− 0.62	1.00	0.07	− 0.81	0.79	− 0.09	− 0.84	− 0.54	0.40	− 0.47	0.60	1

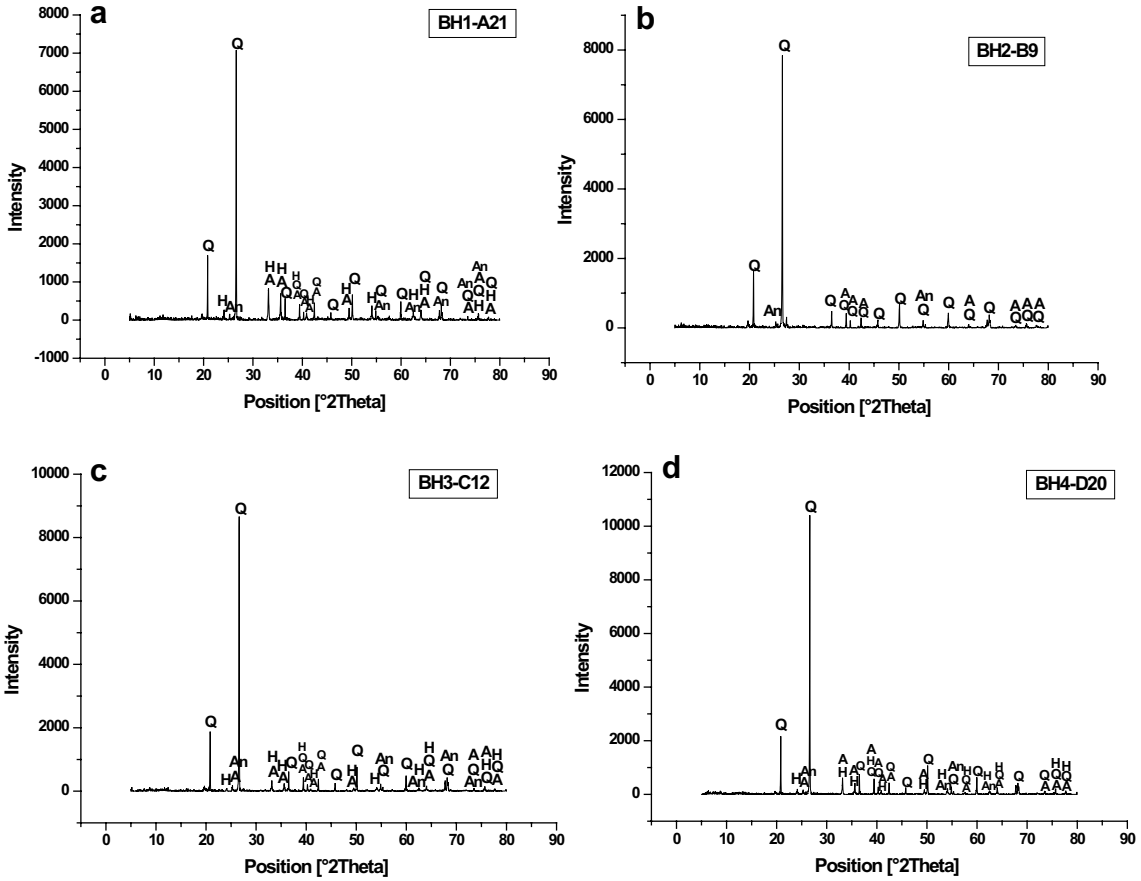

Fig. 7 XRD analysis of representative coal ash samples from each borehole of Samaleswari coal block: **a** BH1 (sample A21), **b** BH2 (sample B9), **c** BH3 (sample C12), and **d** BH4 (sample D20) (Q—Quartz, H—Haemetite, A—Apatite, and An—Anatase)

most clastic sedimentary rocks, including coal deposits, the ratio of Al_2O_3 and TiO_2 has been used efficiently as a provenance indicator in different basins (Hayashi et al. 1997; Dai et al. 2015a, b, 2017). In clastic sedimentary rock derived from mafic, intermediate, and felsic dominant sedimentary source regions, the Al_2O_3/TiO_2 ratios were found to be in the range of 3–8, 8–21, and 21–70, respectively (Hayashi et al. 1997). All the four borehole coal samples of the Samaleswari coal block have Al_2O_3/TiO_2 ratio greater than 21, indicating that the sediment source in the basin was felsic (Fig. 14). The low contents of TiO_2 and MgO in the coals of Samaleswari block also indicate the depletion of Ti and Mg and less mafic minerals, inferring a felsic provenance (Zhang et al. 2020). Moreover, slightly low and negative Eu anomalies (see section 5.1) further support that felsic rock formations have influenced the sediments of the region. The positive correlation of TiO_2 and Al_2O_3 with ∑REE indicates that most of Samaleswari coal's REEs mainly occurred in clay minerals. While a negative correlation of ∑REE with Fe_2O_3 entails REEs in Samaleswari coal may also occur in phosphate and pyrites.

Apart from organic indices, the inorganic constituents have also been used to know the coal-forming environment (Qin et al. 2018). The major oxide ratio [M=(Fe_2O_3+CaO+MgO)/(SiO_2+Al_2O_3)] in coals is one of the significant parameters for studying peat-forming conditions. This ratio discriminates between marine and terrestrial environments during peat deposition. The major oxide ratio (M) value of more than 0.23 entails marine depositional conditions, while less than 0.23 indicates a terrestrial depositional environment (Qin et al. 2018). The M values (less than 0.23) in Samaleswari coal indicate that these coals formed in a terrestrial environment (Table 14). The major oxide concentrations in all four boreholes are more or less similar; therefore, the average values of SiO_2 and (Al_2O_3+K_2O+Na_2O) were plotted on the diagram proposed by Suttner and Dutta (1986), further suggesting that the coal of these boreholes formed under a semi-arid condition (Fig. 15). Moreover, Ce anomalies can give the information about the paleodepositional condition and used as redox indicator. Ce anomaly ˂ 0.78 indicates oxidation condition, and > 0.78 reflects anoxic condition. In the boreholes of Samaleswari coal blocks, the Ce anomaly

Table 13 EPMA point analysis data of the selected coal ash samples acquired from all the four boreholes of Samaleswari coal block

Boreholes name	Point no.	Fe	K	Na	Mg	Al	Si	Ca	Ti	P	La	Ce	Pr	Nd	Sm
CMISW-021	1	5.12	4.32	0.19	0.95	29.68	58.3	0.27	0.65	nd	0.35	nd	0.18	nd	nd
	2	1.95	1.32	0.09	0.72	12.38	79.96	0.4	0.41	nd	nd	nd	0.73	0.23	1.82
	3	5.78	4.93	0.21	1.95	31.15	47.41	2.37	3.47	nd	0.10	1.07	1.17	0.14	0.26
	4	6.52	4.16	0.78	1.45	32.13	50.34	1.71	2.13	nd	0.73	0.04	nd	nd	nd
CMISW-025	1	7.58	6.9	0.6	0.9	32.96	48.78	0.31	0.73	nd	nd	0.14	0.93	0.19	nd
	2	38.72	3.28	1.02	1.12	23.02	31.09	nd	0.83	nd	0.68	0.23	nd	nd	nd
	3	7.32	10.22	0.37	0.69	32.58	45.75	0.72	0.68	nd	0.20	0.29	0.28	nd	0.90
	4	7.12	10.78	0.49	1.23	30.75	46.13	nd	1.51	nd	1.00	0.44	nd	0.56	nd
	5	4.41	2.91	0.24	0.74	33.65	55.05	0.26	2.03	nd	nd	nd	0.34	0.37	nd
	6	1.43	0.8	0.32	0.55	12.74	80.04	0.45	1.74	nd	nd	nd	nd	0.36	1.57
	7	3.23	2.33	0.22	0.62	20.31	65.12	1.16	2.24	nd	1.31	1.48	nd	1.04	0.95
CMISW-27	1	2.44	15.32	0.14	0.61	30.99	45.52	0.06	2.71	nd	nd	0.57	0.61	nd	1.01
	2	2.68	9.86	0.90	0.85	33.21	48.45	0.41	2.54	nd	nd	0.74	0.36	nd	nd
	3	2.37	1.53	nd	0.65	35.92	50.92	0.62	6.31	nd	nd	1.11	0.57	nd	nd
	4	3.44	1.11	nd	0.43	23.67	64.68	0.66	3.54	nd	nd	nd	1.05	0.63	0.77
CMISW-08	1	4.49	0.74	0.39	0.34	23.81	67.33	0.39	1.11	nd	nd	0.75	0.66	nd	nd
	2	3.3	0.58	0.2	0.38	36.21	53.36	0.28	1.31	0.3	0.6	0.14	0.58	1.46	1.29
	3	4.77	1.00	0.6	0.6	33.89	50.48	0.39	6.77	0.21	nd	0.10	0.76	0.43	nd
	4	11.25	0.49	0.74	0.71	30.48	47.08	0.45	6.68	0.07	0.09	1.09	0.87	nd	nd

is $^{>}$ 0.78, except few samples on BH 1in upper sections, indicating that these coal blocks were deposited in anoxic condition.

Implications of exploration of REEs in Samaleswari coal block

Research on exploration and recovery of REE from coal ash is one of the most sought after area, although its augmentation to commercial scale still needs to be determined. Particularly, in Indian scenario, the need to uncover potential REE sources is even more critical knowing the geographical abundance of REEs in Southern Asia. In the present study, two boreholes were found to be potentially rich source of appreciable concentration of La, Ce, Nd, and Y. In particular, the higher concentrations of REEs in BH1 were found to be associated to apatite ore. This means that the isolation of these valuables would be essentially a three-step process: (a) leaching using sulphuric acid, (b) solvent extraction, and (c) precipitation (Battsengel et al. 2018). In BH2, the association of REEs was concluded to be with either monazite or bastnaesite ore. The presence of Yttrium in both boreholes (on an average 48.7 ppm in BH1 and 39.5 ppm in BH2, Tables 9 and 10) indicates the presence of xenotime in coal ash which could be conjoined with the positive correlation with phosphorus in the chosen boreholes (Tables 6 and 7). The lower enrichment of HREE is reflective of the overlap between monazite/bastnaesite and its aluminosilicate host, thus making it economically un-exploitable. With an understanding of the variations in chemical associations, in future, the main focus would be to design efficient and economic strategies to extract REEs from the two enriched boreholes of Samaleswari coal block.

Future work

The present work demonstrated that the two boreholes BH1 and BH2 of Samaleswari coal block are enriched with REEs. The optimization of extraction of these valuables is thus the next crucial step. Therefore, we are planning to optimize the conditions for leaching out these valuables from the coal ash samples and characterize them. Subsequently, optimization of sequential leaching will be performed to delineate the association of HREE and LREE with the inorganic and organic matter the coal samples of this area.

Conclusion

The knowledge of distribution and association of REE in coal samples is necessary to develop efficient strategies for their extraction and utilization. Based on the geochemical and mineralogical studies of the coals from the

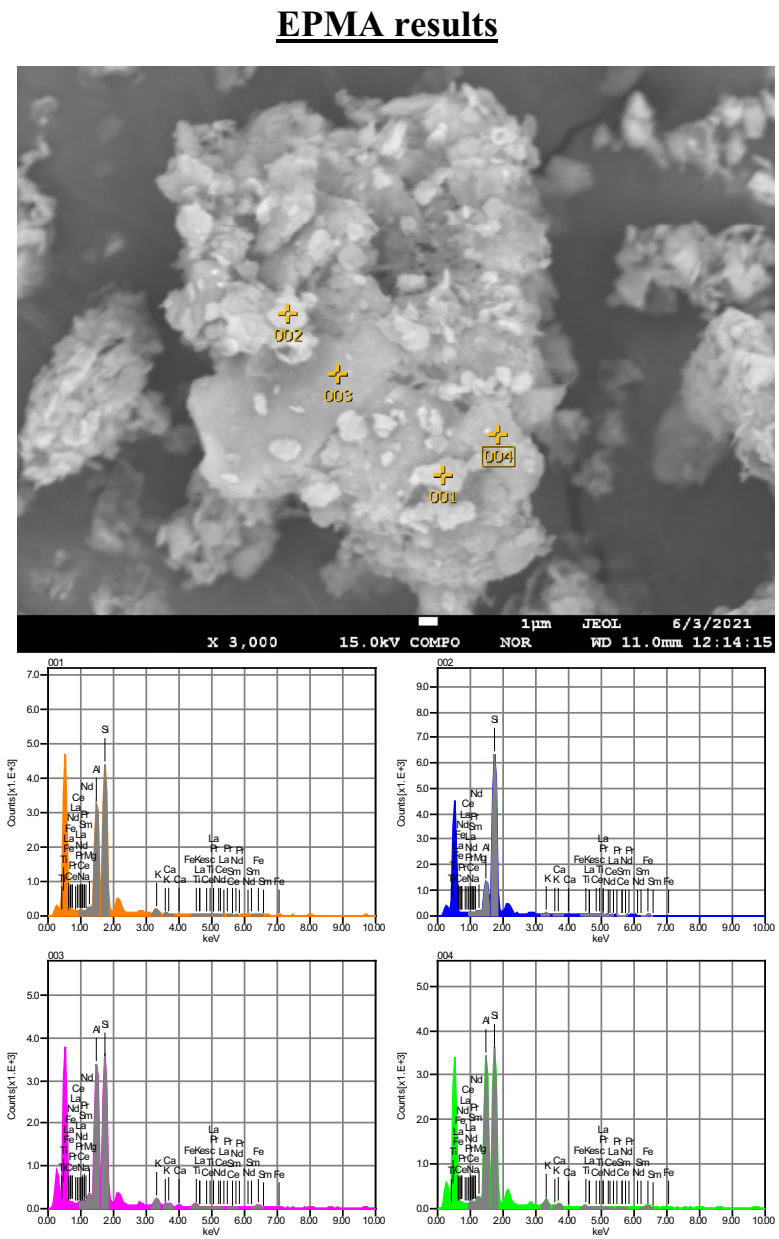

	Fe	K	Na	Mg	Al	Si	Ca	Ti	La	Ce	Pr	Nd	Sm
001	5.12	4.32	0.19	0.95	29.68	58.30	0.27	0.65	0.35	nd	0.18	nd	nd
002	1.95	1.32	0.09	0.72	12.38	79.96	0.40	0.41	nd	nd	0.73	0.23	1.82
003	5.78	4.93	0.21	1.95	31.15	47.41	2.37	3.47	0.10	1.07	1.17	0.14	0.26
004	6.52	4.16	0.78	1.45	32.13	50.34	1.71	2.13	0.73	0.04	nd	nd	nd

Fig. 8 EMPA point analysis results of BH1

Samaleswari coal block, IB valley, Odisha, India, the following conclusions may be drawn:

- The chemical composition of these coals was concluded to be sub-bituminous in rank with a high average ash yield of 49.58% and a low average fixed carbon concentration of 23.46%.
- Eu anomalies are slightly low and negative with high LREE/HREE ratio indicating felsic influence in sedimentation. The ratio of Al_2O_3/TiO_2>21 further sup-

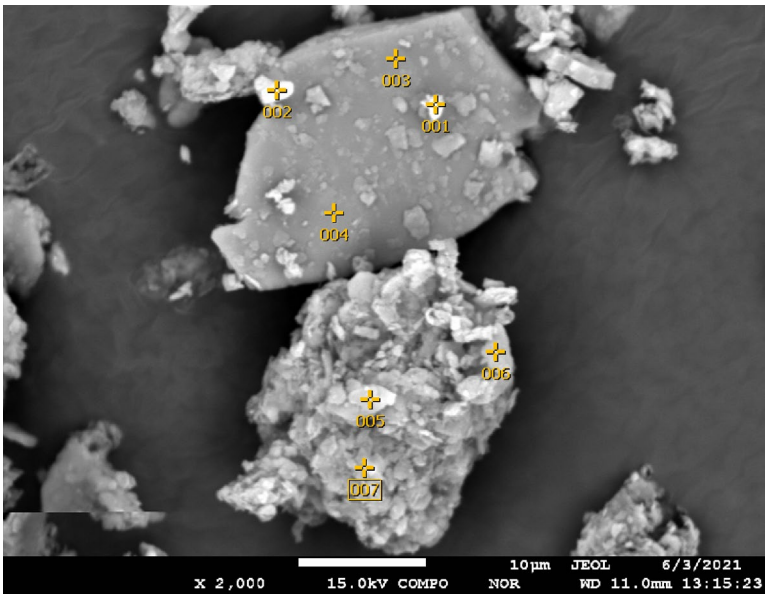

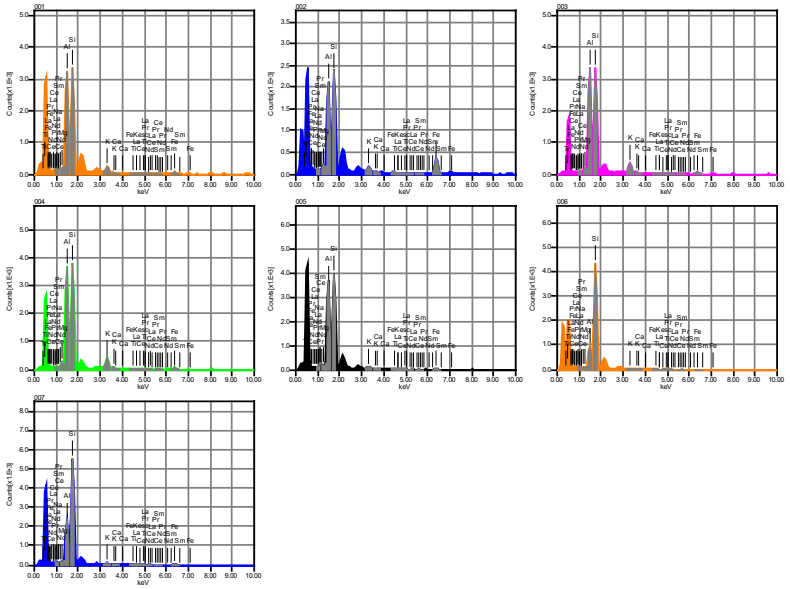

	Fe	K	Na	Mg	Al	Si	Ca	Ti	La	Ce	Pr	Nd	Sm
001	7.58	6.90	0.60	0.90	32.96	48.78	0.31	0.73	nd	0.14	0.93	0.19	nd
002	38.72	3.28	1.02	1.12	23.02	31.09	nd	0.83	0.68	0.23	nd	nd	nd
003	7.32	10.22	0.37	0.69	32.58	45.75	0.72	0.68	0.20	0.29	0.28	nd	0.90
004	7.12	10.78	0.49	1.23	30.75	46.13	nd	1.51	1.00	0.44	nd	0.56	nd
005	4.41	2.91	0.24	0.74	33.65	55.05	0.26	2.03	nd	nd	0.34	0.37	nd
006	1.43	0.80	0.32	0.55	12.74	80.04	0.45	1.74	nd	nd	nd	0.36	1.57
007	3.23	2.33	0.22	0.62	20.31	65.12	1.16	2.24	1.31	1.48	nd	1.04	0.95

Fig. 9 EMPA point analysis results of BH2

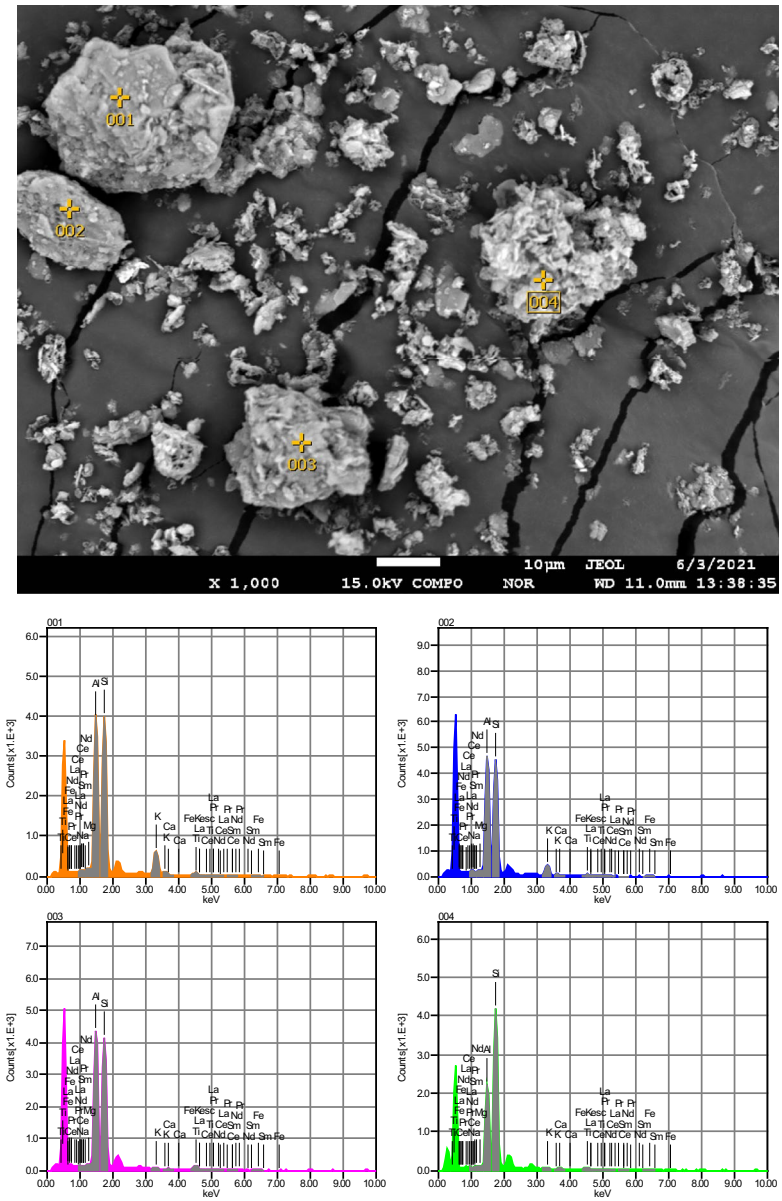

	Fe	K	Na	Mg	Al	Si	Ca	Ti	La	Ce	Pr	Nd	Sm
001	2.44	15.32	0.14	0.61	30.99	45.52	0.06	2.71	nd	0.57	0.61	nd	1.01
002	2.68	9.86	0.90	0.85	33.21	48.45	0.41	2.54	nd	0.74	0.36	nd	nd
003	2.37	1.53	nd	0.65	35.92	50.92	0.62	6.31	nd	1.11	0.57	nd	nd
004	3.44	1.11	nd	0.43	23.67	64.68	0.66	3.54	nd	nd	1.05	0.63	0.77

Fig. 10 EMPA point analysis results of BH3

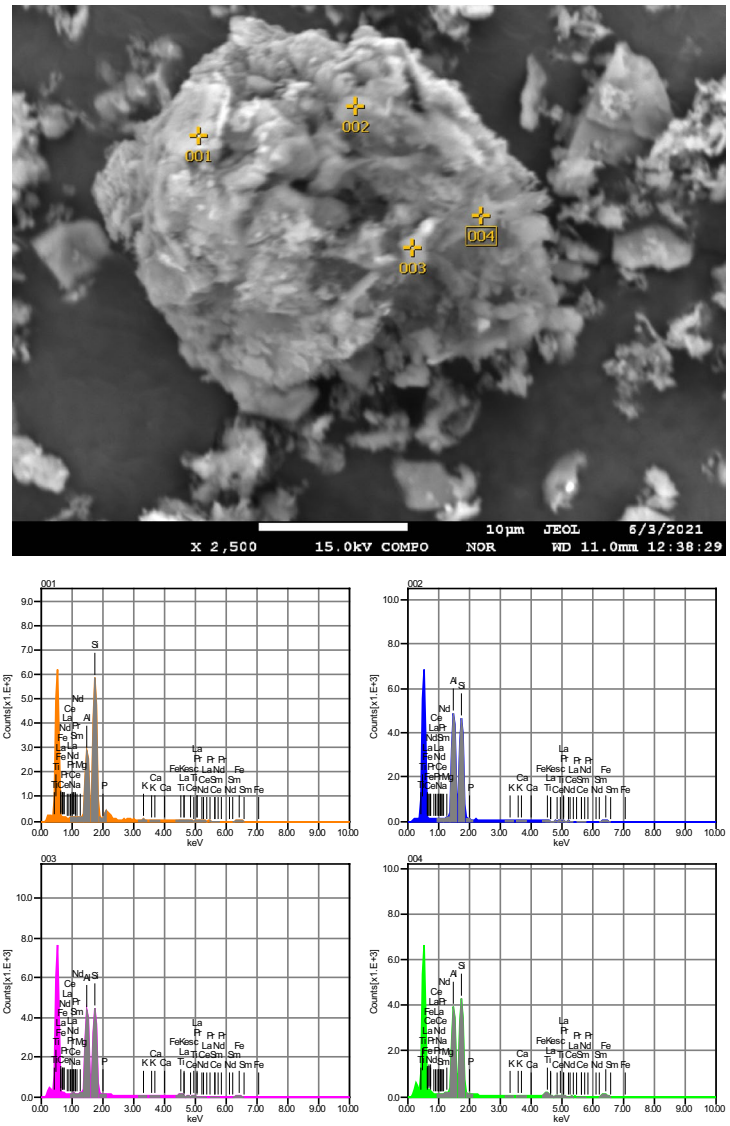

	P	Fe	K	Na	Mg	Al	Si	Ca	Ti	La	Ce	Pr	Nd	Sm
001	nd	4.49	0.74	0.39	0.34	23.81	67.33	0.39	1.11	nd	0.75	0.66	nd	nd
002	0.30	3.30	0.58	0.20	0.38	36.21	53.36	0.28	1.31	0.60	0.14	0.58	1.46	1.29
003	0.21	4.77	1.00	0.60	0.60	33.89	50.48	0.39	6.77	nd	0.10	0.76	0.43	nd
004	0.07	11.25	0.49	0.74	0.71	30.48	47.08	0.45	6.68	0.09	1.09	0.87	nd	nd

Fig. 11 EMPA point analysis results of BH4

ports that the sediment source in the basin was felsic in nature.

- The $(La/Yb)_N$ ratio greater than 1 showed that samples are primarily LREE which are inorganically bound in particular belonged to phosphate and carbonate rocks.
- The concentration of critical rare-earth elements (100–300 ppm) and the C_{outl} (0.7–1.0) indicates that the coal seam from the Samaleswari coal block can be used as a promising source of REE elements.

SEM Micrographs

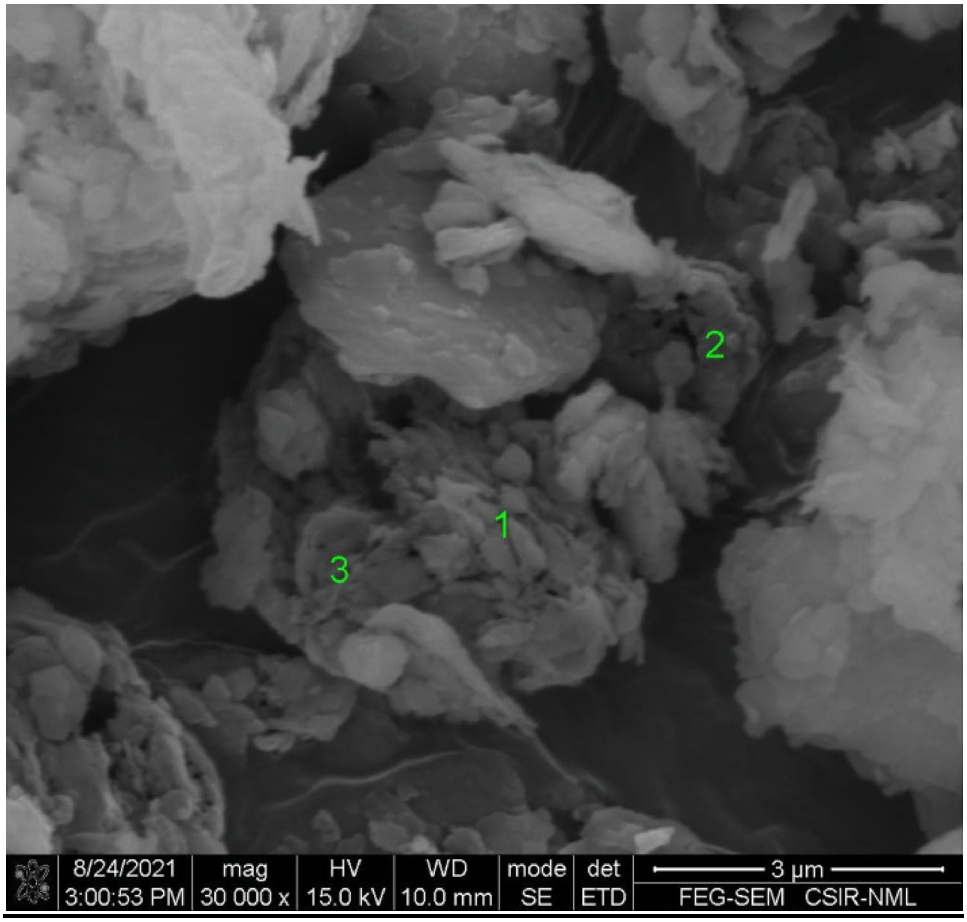

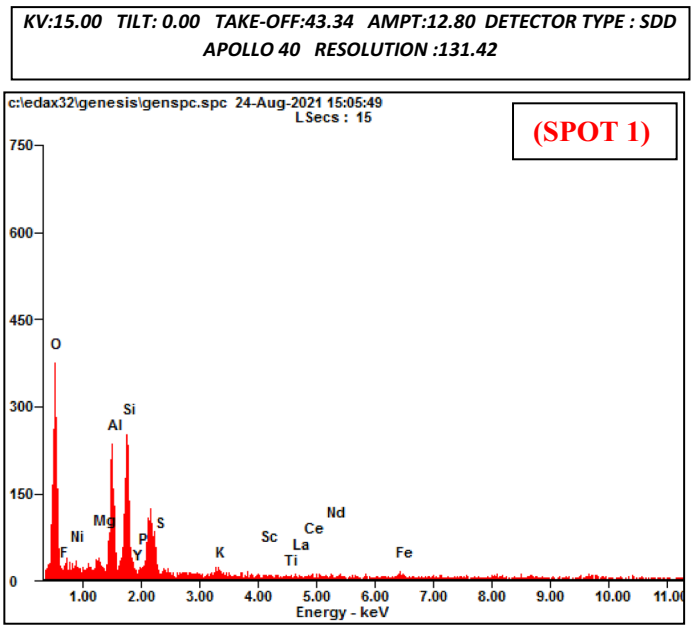

Element	Wt %	At %
O K	34.95	52.46
F K	02.65	03.34
NiL	04.38	01.79
MgK	01.65	01.63
AlK	15.78	14.05
SiK	21.84	18.67
Y L	00.00	00.00
P K	01.92	01.49
S K	01.33	01.00
K K	02.16	01.33
ScK	00.57	00.30
TiK	00.91	00.46
LaL	02.17	00.38
CeL	02.75	00.47
NdL	01.37	00.23
FeK	05.58	02.40

Fig. 12 SEM micrograph of representative sample of BH1

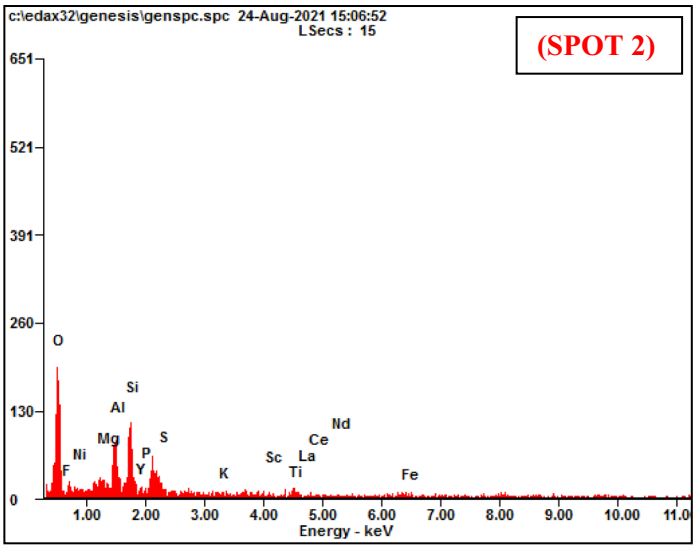

Element	Wt %	At %
O K	39.33	58.36
F K	01.49	01.86
NiL	00.00	00.00
MgK	02.49	02.43
AlK	12.89	11.34
SiK	19.59	16.56
Y L	01.79	00.48
P K	00.88	00.67
S K	02.04	01.51
K K	00.80	00.48
ScK	00.63	00.33
TiK	04.56	02.26
LaL	02.80	00.48
CeL	03.03	00.51
NdL	02.12	00.35
FeK	05.55	02.36

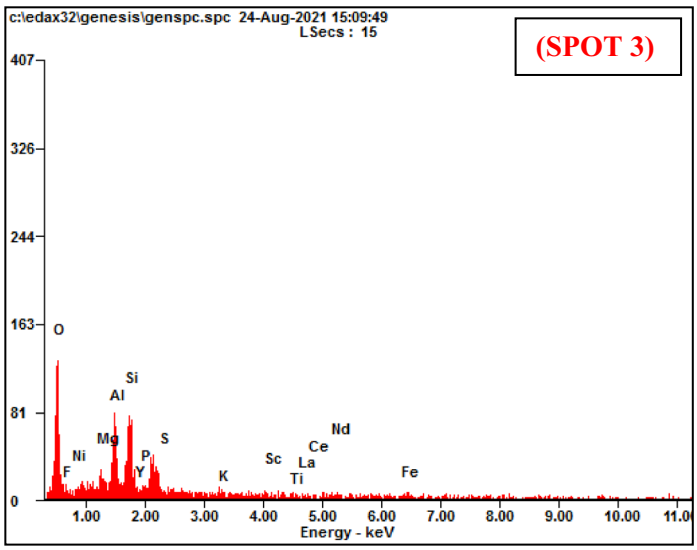

Element	Wt %	At %
O K	31.90	52.48
F K	01.82	02.53
NiL	02.64	01.18
MgK	04.03	04.37
AlK	12.83	12.52
SiK	17.12	16.05
Y L	02.21	00.65
P K	01.55	01.31
S K	00.96	00.79
K K	01.27	00.85
ScK	01.13	00.66
TiK	02.22	01.22
LaL	03.34	00.63
CeL	05.00	00.94
NdL	06.34	01.16
FeK	05.63	02.65

Fig. 12 (continued)

- The concentrations of all HREEs and some LREEs (Sm, Eu, La, and Gd) were found to be significantly higher in BH1, which possessed higher concentration of apatite.
- The presence of titanate mineral bearing REEs was conclusively proven for all four boreholes.
- EPMA point analysis and SEM-EDAX analysis further corroborated the co-existence of REEs in the aluminosilicate glass phase with significant Fe inclusions.
- The major oxide ratio (M‹0.23) value more than entails the terrestrial depositional environment in the basin dur-

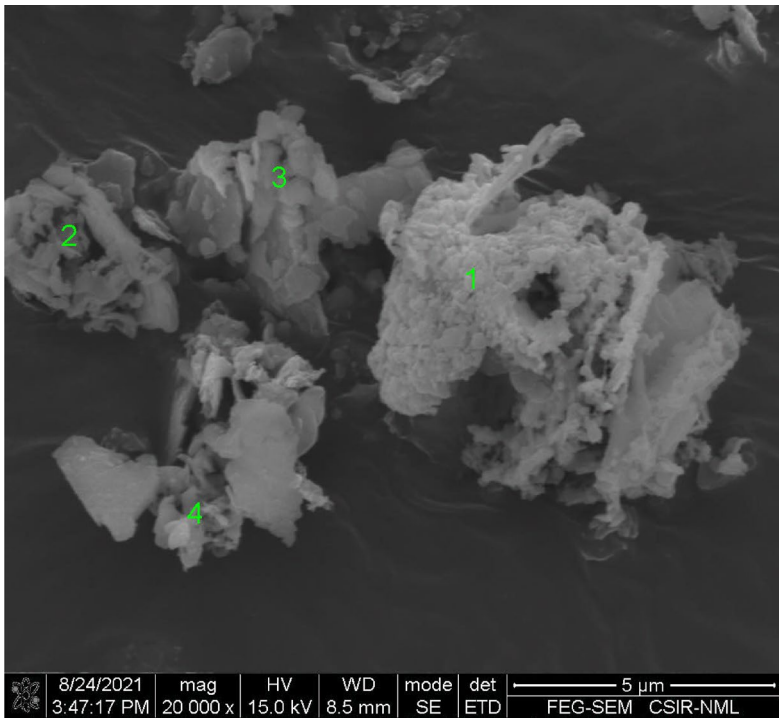

Fig. 13 SEM micrograph of representative sample of BH2

KV:15.00 TILT: 0.00 TAKE-OFF:42.26 AMPT:12.80 DETECTOR TYPE : SDD APOLLO 40 RESOLUTION :131.42

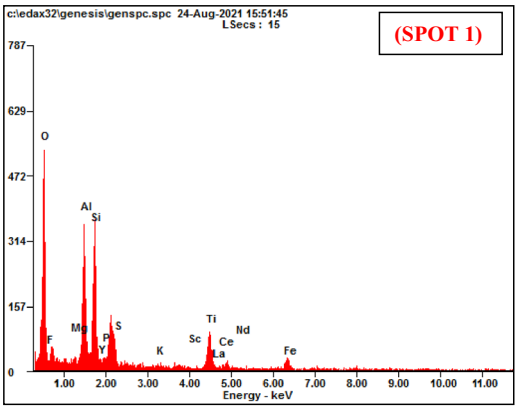

Element	Wt %	At %
O K	36.29	54.63
F K	04.03	05.11
MgK	00.77	00.76
AlK	14.42	12.87
SiK	16.59	14.23
Y L	00.00	00.00
P K	01.08	00.84
S K	00.00	00.00
K K	00.00	00.00
ScK	00.00	00.00
TiK	13.83	06.95
LaL	01.78	00.31
CeL	02.04	00.35
NdL	00.00	00.00
FeK	09.17	03.96

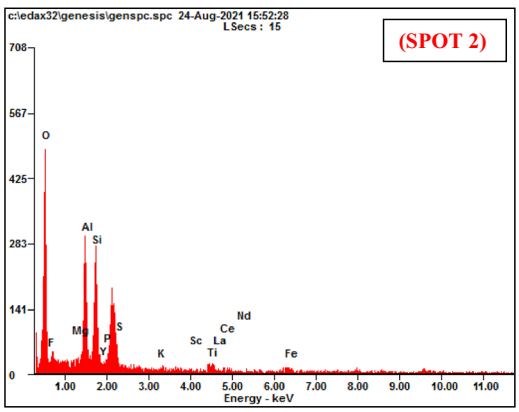

Element	Wt %	At %
O K	37.07	54.97
F K	03.51	04.38
MgK	00.35	00.34
AlK	17.29	15.20
SiK	18.63	15.73
Y L	00.00	00.00
P K	01.88	01.44
S K	01.31	00.97
K K	00.64	00.39
ScK	00.19	00.10
TiK	04.51	02.24
LaL	02.98	00.51
CeL	03.15	00.53
NdL	01.60	00.26
FeK	06.88	02.92

Fig. 13 (continued)

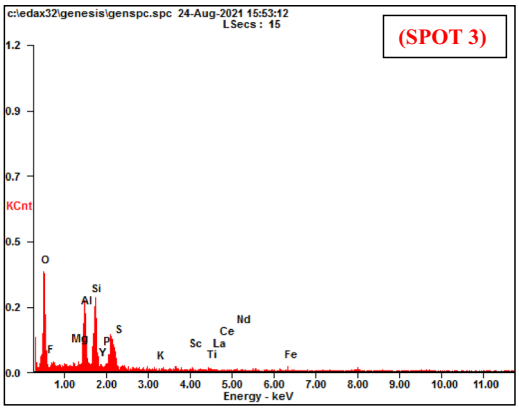

Element	Wt %	At %
O K	37.67	55.43
F K	02.38	02.95
MgK	00.63	00.61
AlK	16.80	14.66
SiK	21.20	17.77
Y L	00.65	00.17
P K	02.71	02.06
S K	01.12	00.82
K K	00.39	00.24
ScK	00.60	00.31
TiK	02.59	01.27
LaL	02.71	00.46
CeL	01.14	00.19
NdL	03.51	00.57
FeK	05.90	02.49

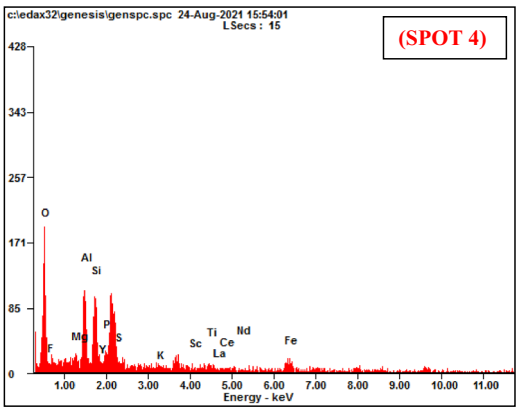

Element	Wt %	At %
O K	27.95	48.14
F K	02.76	04.01
MgK	01.46	01.66
AlK	13.11	13.38
SiK	14.56	14.29
Y L	00.57	00.18
P K	03.52	03.13
S K	01.28	01.10
K K	00.47	00.33
ScK	01.03	00.63
TiK	03.82	02.20
LaL	05.83	01.16
CeL	04.22	00.83
NdL	02.04	00.39
FeK	17.38	08.57

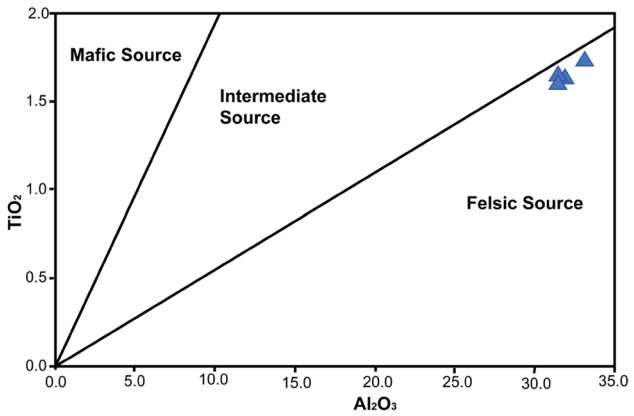

Fig. 14 Plot of TiO_2 versus Al_2O_3 form average concentration of four bore holes of Samaleswari coals (Imchen et al 2014)

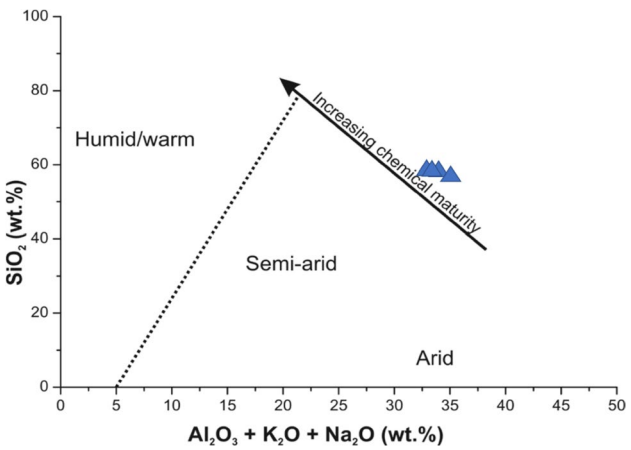

Fig. 15 Plot of SiO_2 versus $(Al_2O_3 + K_2O + Na_2O)$ showing paleoclimate condition during sedimentation (Suttner and Dutta 1986)

Table 14 The major oxide ratio for studying peat-forming conditions

Borehole	Sample	$Fe_2O_3 + CaO + MgO / SiO_2 + Al_2O_3$
BH-1	A1	0.06
	A2	0.10
	A3	0.04
	A4	0.05
	A5	0.06
	A6	0.05
	A7	0.08
	A8	0.06
	A9	0.05
	A10	0.06
	A11	0.05
	A12	0.06
	A13	0.07
	A14	0.14
	A15	0.09
	A16	0.09
	A17	0.05
	A18	0.06
	A19	0.16
	A20	0.14
	A21	0.18
	A22	0.07
	A23	0.07
	A24	0.02
BH-2	B1	0.06
	B2	0.05
	B3	0.05
	B4	0.07
	B5	0.04
	B6	0.04
	B7	0.11
	B8	0.05
	B9	0.06
	B10	0.07
	B11	0.07
	B12	0.07
	B13	0.33
	B14	0.10
	B15	0.09
	B16	0.06
	B17	0.02
BH-3	C1	0.05
	C2	0.06
	C3	0.09
	C4	0.10
	C5	0.09
	C6	0.04
	C7	0.06
	C8	0.05
	C9	0.05
	C10	0.06
	C11	0.04
	C12	0.04
	C13	0.07
	C14	0.06
	C15	0.04
	C16	0.04
	C17	0.08
	C18	0.08
	C19	0.06
	C20	0.10
	C21	0.09
	C22	0.06
	C23	0.04
	C24	0.07
BH-4	D1	0.07
	D2	0.05
	D3	0.06
	D4	0.05
	D5	0.04
	D6	0.11
	D7	0.05
	D8	0.07
	D9	0.06
	D10	0.06
	D11	0.06
	D12	0.07
	D13	0.09
	D14	0.11
	D15	0.12
	D16	0.06
	D17	0.07
	D18	0.07
	D19	0.03
	D20	0.03

ing coal formation and the major oxide plot suggests that the coal of these boreholes formed under a semi-arid condition.

Supplementary Information The online version contains supplementary material available at https://doi.org/10.1007/s12665-023-10777-7.

Acknowledgements The authors would like to extend their gratitude to Director, CSIR-NML for allowing them to carry out and publish this work. We would like to thank CMPDIL (Coal India Ltd.) for the coal samples.

Author contributions 1. SK: Conceptualization, Data curation, Formal analysis, Writing – original draft2. TR: Review & editing, Formal analysis3. SC: Writing – original draft, review & editing, Formal analysis, Interpretation4. AK: Manuscript writing, review & editing in the original draft, illustrations, Interpretation4. MA: Formal analysis, Review & edit the original draft5. AM: Review & edit the original draft, Formal analysis6. RK: Review & edit the original draft, Formal analysis7. SC: Project administration, Investigation, Supervision. Conceptualization.

Funding This study was funded by National Metallurgical Laboratory.

Data availability statement The data could be made available upon request to the authors.

Declarations

Competing interests The authors declare no competing interests.

Conflict of interest All authors declare that they have no conflict of interest.

References

Abaka-Wood GB, Ehrig K, Addai-Mensah J, Skinner W (2022) Recovery of rare earth elements minerals from iron-oxide-silicaterich tailings: research review. Eng 2022(3):259–275

Bandopadhyay AK, Chatterjee R (2006) Proceedings 23rd Annual International Pittsburgh Coal Conference, Coal Chemistry, Geosciences and Resources: Mineral Matter, Coal, Ash, Coal Combustion, 44.

Banerjee R, Mohanty A, Chakravarty S, Chakladar S, Biswas P (2021) A single-step process to leach out rare earth elements from coal ash using organic carboxylic acids. Hydrometallurgy 201:105575–105590

Battsengel A, Batnasan A, Narankhuu A, Haga K, Watanabe Y, Shibayama A (2018) Recovery of light and heavy rare earth elements from apatite ore using sulphuric acid leaching, solvent extraction and precipitation. Hydrometallurgy 179:100–109

Bhattacharjee U, Kandpal TC (2002) Potential of fly ash utilisation in India. Energy 27:151

Birk D, White JC (1991) Rare earth elements in bituminous coals and underclays of the Sydney Basin, Nova Scotia: element sites, distribution, mineralogy. Int J Coal Geol 19:219–251

Dai S, Finkelman RB (2018) Coal as a promising source of critical elements: progress and future prospects. Int J Coal Geol 186:155–164

Dai S, Seredin VV, Ward CR, Hower JC, Xing Y, Zhang W, Song W, Wang P (2015a) Enrichment of U-Se–Mo–Re–V in coals preserved within marine carbonate successions: geochemical and mineralogical data from the Late Permian guiding coalfield, Guizhou, China. Miner Depos 50:159–186

Dai S, Yang J, Ward CR, Hower JC, Liu H, Garrison TM, French D, O'Keefe JMK (2015b) Geochemical and mineralogical evidence for a coal-hosted uranium deposit in the Yili Basin, Xinjiang, northwestern China. Ore Geol Rev 70:1–30

Dai S, Graham IT, Ward CR (2016a) A review of anomalous rare earth elements and yttrium in coal. Int J Coal Geol 159:82–95

Dai S, Xie P, Jia S, Ward CR, Hower HC, Yan X, French D (2017) Enrichment of U-Re-V-Cr-Se and rare earth elements in the Late Permian coals of the Moxinpo Coalfield, Chongqing, China: genetic implications from geochemical and mineralogical data. Ore Geol Rev 80:1–17

Dai S, Guo W, Nechaev VP, French D, Ward CR, Spiro BF, Finkelman RB (2018) Modes of occurrence and origin of mineral matter in the Palaeogene coal (No. 19–2) from the Hunchun Coalfield, Jilin Province, China. Int J Coal Geol 189:94–110

Eskenazy GM (2009) Trace elements geochemistry of the Dobrudza coal basin, Bulgaria. Int J Coal Geol 78:192–200

Firman F, Haya A (2021) Study on the potential rare earth elements in coal combustion product from Banjarsari power plant, South Sumatera. IOP Conf Ser: Mater Sci Eng 1125:012003

Franus W, Wiatros-Motyka MM, Wdowin M (2015) Coal fly ash as a resource for rare earth elements. Environ Sci Pollut Res 22:9464–9474

Geological Survey of India (2019) Indian coal and lignite resources-2019. Natural Energy Resources Mission-II B, Government of India

Hayashi KI, Fujisawa H, Holland HD, Ohmoto H (1997) Geochemistry of 1.9 Ga sedimentary rocks from northeastern Labrador, Canada. Geochim Cosmochim Acta 61:4115–4137

Hood MM, Taggart RK, Smith RC, Hsu-Kim H, Henke KR, Graham U, Groppo JG, Unrine JM, Hower JC (2017) Rare earth element distribution in fly ash derived from the fire clay coal, Kentucky. Coal Combust Gasif Prod 9:22–23

Hower JC, Groppo JG, Joshi P, Dai S, Moecher DP, Johnston MN (2013) Location of cerium in coal combustion fly ashes: implications for recovery of lanthanides. Coal Combust Gasif Prod 5:73–78

Hower JC, Eble CF, Dai S, Belkin HE (2016) Distribution of rare earth elements in eastern Kentucky coals: indicators of multiple modes of enrichment? Int J Coal Geol 160:73–81

Imchen W, Thong GT, Pongen T (2014) Provenance, tectonic setting and age of the sediments of the Upper Disang formation in the Phek district, Nagaland. J Asia Earth Sci 88:11–27

Indian Minerals yearbook (2019) Part III: mineral reviews, 58th Edition, Govt. Of India, Ministry of Mines, Nagpur.

Ketris MP, Yudovich YaE (2009) Estimations of Clarkes for carbonaceous biolithes: world averages for trace element contents in black shales and coals. Int J Coal Geol 78:135–148

King PL, Sham TK, Gordon RA, Dyar MD (2012) Microbeam X-ray analysis of Ce3+/Ce4+ in Ti-rich minerals: a case study with titanite (sphene) with implications for multivalent trace element substitution in minerals. Am Miner 98:110–119

Kolker A, Scott C, Hower JC, Vazquez JA, Lopano CL, Dai S (2017) Distribution of rare earth elements in coal combustion fly ash, determined by SHRIMP-RG ion microprobe. Int J Coal Geol 184:1–10

Kortenski J, Bakardjiev S (1993) Rare earth and radioactive elements in some coals from the Sofia, Svoge and Pernik Basins, Bulgaria. Int J Coal Geol 22:237–246

Lin R, Bank TL, Roth EA, Granite EJ, Soong Y (2017) Organic and inorganic associations of rare earth elements in central Appalachian coal. Int J Coal Geol 179:295–301

Manjrekar VD, Choudhury V, Gautam KVVS (2006) Coal. In: Mahalik NK (ed) Geology and mineral resources of Orissa. Society of Geoscientists and Allied Technologist, Bhubaneswar, pp 205–226

Mayfield DB, Lewis AS (2013) Environmental review of coal ash as a resource for rare earth and strategic elements. Proceedings of

the 2013 World of Coal Ash (WOCA) Conference, Lexington, KY, USA
Mishra V, Bhowmick T, Chakravarty S, Varma AK, Sharma M (2016) Influence of coal quality on combustion behaviour and mineral phases transformations. Fuel 186:443–455
Mohanty A, Das S, Vijayan V, Sengupta D, Saha S (2003) Geochemical studies of monazite sands of Chhatrapur beach placer deposit of Orissa, India by PIXE and EDXRF method. Nucl Instrum Methods Phys Res, Sect B 211:145–154
Mukherjee S, Srivastava SK (2006) Minerals transformations in Northeastern Region coals of India on heat treatment. Energy Fuels 20:1089–1096
Oreskes N, Einaudi MT (1990) Origin of rare earth element-enriched hematite breccias at the Olympic Dam Cu-U-Au-Ag deposit, Roxby Downs, South Australia. Econ Geol 85:1–28
Qin S, Gao K, Sun Y, Wang J, Zhao C, Li S, Lu Q (2018) Geochemical characteristics of rare-metal, rare-scattered, and rare-earth elements and minerals in the late Permian coals from the Moxinpo mine, Chongqing, China. Energy Fuels 32:3138–3151
Rautenbach R, Matjie R, Strydom C, Bunt J (2021) Transformation of inherent and extraneous minerals in feed coals of commercial power stations and their density-separated fractions. Energy Geosci 2:136–147
Saha D, Chakravarty S, Shome D, Basariya MR, Kumari A, Kundu AK, Chatterjee D, Adhikari J, Chatterjee D (2016) Distribution and affinity of trace elements in Samaleswari coal, Eastern India. Fuel 181:376–388
Saha D, Chatterjee D, Chakravarty S, Mazumder M (2018) Trace element geochemistry and mineralogy of coal from Samaleswari open cast coal block (S-OCB), Eastern India. Phys Chem Earth, Parts a/b/c 104:47–57
Saikia BK, Hower JC, Islam N, Sharma A, Das P (2021) Geochemistry and petrology of coal and coal fly ash from a thermal power plant in India. Fuel 291:120122
Senapaty A, Behera P (2015) Stratigraphic control of petrography and chemical composition of the lower Gondwana coals, Ib-valley coalfield, Odisha, India. J Geosci Environ Prot 03:56–66
Seredin VV (1996) Rare earth element-bearing coals from the Russian Far East deposits. Int J Coal Geol 30:101–129
Seredin VV (1998) Rare earth mineralization in Late Cenozoic explosion structures (Khankai massif, Primorskii Krai, Russia). Geol Ore Depos 40:357–371
Seredin VV, Dai S (2012) Coal deposits as potential alternative sources for lanthanides and yttrium. Int J Coal Geol 94:67–93
Seredin VV, Dai S, Sun Y, Chekryzhov IY (2013) Coal deposits as promising sources of rare metals for alternative power and energy-efficient technologies. Appl Geochem 31:1–11
Singh PK, Singh GP, Singh MP, Naik AS (2013) The petrology of coals from the Rampur seam-IV and the Lajkura seam, Ib river coalfield, Mahanadi Valley, Orissa, India. Energy Sources, Part A 35:1681–1690
Sorokin AP, Konyushok AA, Ageev OA, Zarubina NV, Ivanov VV, Wang J (2019) Distribution of rare earth and selected trace elements in combustion products of Yerkovetskoe brown coal deposit (Amur Region, Russia). Energy Explor Exploit 37:1721–1736
Stuckman MY, Lopano CL, Granite EJ (2018) Distribution and speciation of rare earth elements in coal combustion by-products via synchrotron microscopy and spectroscopy. Int J Coal Geol 195:125–138
Suttner LJ, Dutta PK (1986) Alluvial sandstone composition and paleoclimate, I. Framework mineralogy. J Sediment Res 56:329–345
Tatar A, Alipour-Asll M (2020) Geochemistry of major, trace and rare earth elements in coals from the Tazareh mine, eastern Alborz coalfield, NE Iran. Geochem: Explor Environ, Anal 20:381–398
Taylor SR, McLennan SM (1985) The continental crust: its composition and evolution, United States.
Tobia FH, Al-Jaleel HS, Ahmad IN (2019) Provenance and depositional environment of the Middle-Late Jurassic shales, northern Iraq. Geosci J 23:747–765
U.S. Department of Energy (2017) National energy technology laboratory
Varga G (2007) The structure of kaolinite and metakaolinite. Epitoanyag 59:4–8
Wang W, Qin Y, Sang S, Zhu Y, Wang C, Weiss DJ (2008) Geochemistry of rare earth elements in a marine influenced coal and its organic solvent extracts from the Antaibao mining district, Shanxi, China. Int J Coal Geol 76:309–317
Wang X, Tang Y, Jiang Y, Xie P, Zhang S, Chen Z (2017) Mineralogy and geochemistry of an organic- and V-Cr-Mo-U-rich siliceous rock of Late Permian age, western Hubei Province, China. Int J Coal Geol 172:19–30
Wang Z, Dai S, Zou J, French D, Graham IT (2019) Rare earth elements and yttrium in coal ash from the Luzhou power plant in Sichuan, Southwest China: concentration, characterization and optimized extraction. Int J Coal Geol 203:1–14
Wang L, Lv D, Hower JC, Zhang Z, Raji M, Tang J, Liu Y, Gao J (2022) Geochemical characteristics and paleoclimate implication of Middle Jurassic coal in the Ordos Basin, China. Ore Geol Rev 144:104848
Ward CR (2002) Analysis and significance of mineral matter in coal seams. Int J Coal Geol 50:135–168
Ward CR (2016) Analysis, origin and significance of mineral matter in coal: an updated review. Int J Coal Geol 165:1–27
Yang J, Zhao Y, Zyryanov V, Zhang J, Zheng C (2014) Physical–chemical characteristics and elements enrichment of magnetospheres from coal fly ashes. Fuel 135:15–26
Zhang XL, Gao ZQ, Fan TL, Xue JQ, Li WH, Zhang H, Cao FD (2020) Element geochemical characteristics, provenance attributes, and paleosedimentary environment of the Paleogene strata in the Lenghu area, northwestern Qaidam Basin. J Petrol Sci Eng 195:107750
Zhao L, Ward CR, French D, Graham IT (2013) Mineralogical composition of Late Permian coal seams in the Songzao Coalfield, southwestern China. Int J Coal Geol 116–117:208–226
Zhao L, Dai S, Graham IT, Li X, Liu H, Song X, Hower JC, Zhou Y (2017) Cryptic sediment-hosted critical element mineralization from eastern Yunnan Province, southwestern China: mineralogy, geochemistry, relationship to Emeishan alkaline magmatism and possible origin. Ore Geol Rev 80:116–140
Zheng L, Liu G, Chou CL, Qi C, Zhang Y (2007) Geochemistry of rare earth elements in Permian coals from the Huaibei coalfield, China. J Asian Earth Sci 31:167–176